格子QCDによる有限温度相転移の研究

格子QCDによる有限温度相転移の研究

課題番号　08640350

平成8年度～平成9年度科学研究費補助金（基盤研究C(2)）
研究成果報告書

1998年9月

研究代表者　青　木　慎　也
（筑波大学物理学 助教授）

格子ＱＣＤによる有限温度相転移の研究

課題番号０８６４０３５０

平成８年度～平成９年度科学研究費補助金（基盤研究Ｃ（２））研究成果報告書

１９９８年9月

研究代表者　青木　慎也
（筑波大学物理学　助教授）

平成８年度～平成９年度科学研究費補助金（基盤研究Ｃ（２））

1. 課題番号　０８６４０３５０

2. 研究課題　格子ＱＣＤによる有限温度相転移の研究

3. 研究組織

研究代表者：　青木　慎也　（筑波大学物理学系助教授）

4. 研究経費

平成８年度	１、５００　千円
平成９年度	９００　千円
計	２、４００　千円

研究発表（本報告書収録論文のは＊を付す）

（1）学会誌等

1.1* Structure of critical lines in quenched lattice QCD with the Wilson quark action
S. Aoki, T. Kaneda and A. Ukawa
Physical Review D 56 (1997) 1808-1811

1.2* Scaling study of the two-flavor chiral transition with Kogut-Susskind quark action
S. Aoki, M. Fukugita, S. Hashimoto, N. Ishizuka, Y. Iwasaki, K. Kanaya, Y.Kuramasi, M. Okawa, A. Ukawa and T. Yoshie
Physical Review D 57 (1997) 3910-3922

1.3* Chiral zero modes on the domain-wall mode in 4+1 dimensions
S. Aoki and K. Nagai
Physical Review D 56 (1997) 1121-1130

1.4* Domain wall fermions with Majorana coupling
S. Aoki, K. Nagai and S. V. Zenkin
Nuclear Physics B 508 (1988) 715-727

1.5* One loop calculation in lattice QCD with domain-wall quarks
S. Aoki and Y. Taniguchi
Physical Rev. D (in press)

1.6* The doma-wall model in an asymptotic-free dynamics
S. Aoki and K. Nagai
Physcal Rev. D 58 (1998) 45002

1.7* Kaon B parameter from quenched Lattice QCD
S. Aoki, M. Fukugita, S. Hashimoto, N. Ishizuka, Y. Iwasaki, K. Kanaya, Y. Kuramasi, H. Mino, M. Okawa, A. Ukawa and T. Yoshie
Physical Review Letters 80 (1998) 5271-5274

1.8* Lattice QCD calculation of the Kaon B parameter with the Wilson Quark Action
S. Aoki, M. Fukugita, S. Hashimoto, N. Ishizuka, Y. Iwasaki, K. Kanaya, Y. Kuramasi, M. Okawa, A. Ukawa and T. Yoshie
Physical Review Letters 81 (1998) 1778-1781.

1.9* B meson decay constant from quenched lattice QCD
S. Aoki, M. Fukugita, S. Hashimoto, N. Ishizuka, Y. Iwasaki, K. Kanaya, Y. Kuramasi, M. Okawa, A. Ukawa and T. Yoshie
Physical Review Letters 80 (1998) 5711-5715

1.10* $K^+ \to \pi^+\pi^-$ decay amplitude in quenched lattice QCD
S. Aoki, M. Fukugita, S. Hashimoto, N. Ishizuka, Y. Iwasaki, K. Kanaya, Y. Kuramasi, M. Okawa, A. Ukawa and T. Yoshie
Physical Review D 58 (1998) 54503

（2）国際会議報告

2.1* Finite-temperature phase structure of lattice QCD with the Wilson quark action for two and four lavors
S. Aoki, T. Kaneda, A. Ukawa and T. Umemura
Nuclear Physics B(Proc. Suppl.) 53 (1997) 438-441

2.2* Scaling analysis of chiral phase transition for two flavors of Kogut-Susskind quarks
S. Aoki, M. Fukugita, S. Hashimoto, N. Ishizuka, Y. Iwasaki, K. Kanaya, Y. Kuramasi, H. Mino, M. Okawa, A. Ukawa and T. Yoshie
Nuclear Physics B(Proc. Suppl.) 60A (1998) 188-194

2.3* Phase structure of lattice QCD with Wilson fermion at finite temperature
S. Aoki
Nuclear Physics B(Proc. Suppl.) 60A (1998) 206-219

2.4* Finite-temperature chiral transition in QCD with the Wilson quark action
S. Aoki, Y. Iwasaki, K. Kanaya, S. Kaya A. Ukawa and T. Yoshie
Nuclear Physics B(Proc. Suppl.) 63 (1998) 397-399

2.5* Two-flavor chiral phase transition in lattice QCD with the Kogut-Susskind quark action
S. Aoki, M. Fukugita, S. Hashimoto, N. Ishizuka, Y. Iwasaki, K. Kanaya, Y. Kuramasi, H. Mino, M. Okawa, A. Ukawa and T. Yoshie
Nuclear Physics B(Proc. Suppl.) 63 (1998) 403-405

2.6 One loop calculation of QCD with domain-wall quarks
S. Aoki and Y. Taniguchi
Nuclear Physics B(Proc. Suppl.) 63 (1998) 290-292

2.7 Lattice fermion with Majorana couplings
S. Aoki, K. Nagai and S. V. Zenkin
Nuclear Physics B(Proc. Suppl.) 63 (1998) 602-604

2.8 The Kaon B-parameter with the Wilson quark action using chiral Ward identities
S. Aoki, M. Fukugita, S. Hashimoto, N. Ishizuka, Y. Iwasaki, K. Kanaya, Y. Kuramasi, M. Okawa, A. Ukawa and T. Yoshie
Nuclear Physics B(Proc. Suppl.) 60A (1998) 67-76

2.9 The light quark masses with the Wilson quark action using chiral Ward identities
S. Aoki, M. Fukugita, S. Hashimoto, N. Ishizuka, Y. Iwasaki, K. Kanaya, Y. Kuramasi, M. Okawa, A. Ukawa and T. Yoshie
Nuclear Physics B(Proc. Suppl.) 63 (1998) 275-277

2.10 B meson decay constant with the Wilson and clover heavy quark actions
S. Aoki, M. Fukugita, S. Hashimoto, N. Ishizuka, Y. Iwasaki, K. Kanaya, Y. Kuramasi, M. Okawa, A. Ukawa and T. Yoshie
Nuclear Physics B(Proc. Suppl.) 63 (1998) 281-283

2.11 $K^+ \to \pi^+\pi^-$ decay amplitude in quenched lattice QCD
S. Aoki, M. Fukugita, S. Hashimoto, N. Ishizuka, Y. Iwasaki, K. Kanaya, Y. Kuramasi, M. Okawa, A. Ukawa and T. Yoshie
Nuclear Physics B(Proc. Suppl.) 63 (1998) 284-286

2.12 Pertrubative renormalization parameters fpr heavy quarks
K-I. Ishikawa, S. Aoki, S. Hashimoto, H. Matsufuru, T. Onogi and N. Yamada
Nuclear Physics B(Proc. Suppl.) 63 (1998) 344-346

2.13 Results from quenched B_K from JLQCD
S. Aoki, M. Fukugita, S. Hashimoto, N. Ishizuka, Y. Iwasaki, K. Kanaya, Y. Kuramasi, M. Okawa, A. Ukawa and T. Yoshie
Nuclear Physics B(Proc. Suppl.) 63 (1998) 356-358

2.14 Heavy quark mass dependence of semileptonic form factors for B decays
S. Aoki, M. Fukugita, S. Hashimoto, K-I. Ishikawa, N. Ishizuka, Y. Iwasaki, K. Kanaya, Y. Kuramasi, H. Matsufuru, M. Okawa, A. Ukawa N. Yamada and T. Yoshie
Nuclear Physics B(Proc. Suppl.) 63 (1998) 380-382

2.15 CP-PACS results for quenched QCD spectrum with the Wilson action
S. Aoki, G. Boyd, R. Burkhalter, S. Hashimoto, N. Ishizuka, Y. Iwasaki, K. Kanaya, Y. Kuramashi, M. Okawa, A. Ukawa and T. Yoshie
Nuclear Physics B(Proc. Suppl.) 60A (1998) 14-25

2.16 Full QCD simulation on CP-PACS
S. Aoki, G. Boyd, R. Burkhalter, S. Hashimoto, N. Ishizuka, Y. Iwasaki, K. Kanaya, T. Kaneko, Y. Kuramashi, M. Okawa, A. Ukawa and T. Yoshie
Nuclear Physics B(Proc. Suppl.) 60A (1998) 335-340

2.17 CP-PACS result for quecnhed light hadron spectrum
S. Aoki, G. Boyd, R. Burkhalter, S. Hashimoto, N. Ishizuka, Y. Iwasaki, K. Kanaya, T. Kaneko, Y. Kuramashi, M. Okawa, A. Ukawa and T. Yoshie
Nuclear Physics B(Proc. Suppl.) 63 (1998) 161-163

2.18 Hadron spectroscopy and static quark potential in full QCD: A comparison of improved actions on the CP-PACS
S. Aoki, G. Boyd, R. Burkhalter, S. Hashimoto, N. Ishizuka, Y. Iwasaki, K. Kanaya, T. Kaneko, Y. Kuramashi, M. Okawa, A. Ukawa and T. Yoshie
Nuclear Physics B(Proc. Suppl.) 63 (1998) 221-226

研究成果概要

格子ＱＣＤの数値計算ではウィルソン・フェルミオンと呼ばれる定式化を用いるが、この方法はカイラル対称性をあらわに壊してしまうために相構造そのものがよく理解されていなかった。代表研究者は以前の研究で、ウィルソン・フェルミオンの格子ＱＣＤに存在するゼロ質量のパイ中間子をパリティ・フレーバー対称性を破る相転移に付随するゼロ・モードと解釈できることを発見し、クォークのフレーバー数が２の場合の有限温度の相構造を明らかにした。本研究の目的は、フレーバー数が２の場合の結果を基に、フレーバー数を変えた場合や格子作用を変更した場合に対して数値計算を行い、格子ＱＣＤの有限温度での相構造の普遍的な性質を明らかにすることである。今回交付された科学研究費補助金を基にした研究で我々が得た成果の概略を以下にまとめる。なお、[1.1]などは巻頭に挙げた論文リストの番号であり、*のついた論文は本成果報告に収録してある。

（１）パリティ・フレーバー対称性の自発的破れ

ウィルソン・フェルミオンの相構造を理解する上で鍵となるのはパリティ・フレーバー対称性の自発的破れである。フレーバー数が２の場合の相構造は、パイ中間子の質量を計算することで調べられてきたが、そこではパリティ・フレーバー対称性の自発的破れの存在が前提とされていた。もちろん、解析的な計算やクエンチ近似での数値計算の結果はパリティ・フレーバー対称性が自発的に破れる相の存在を強く示唆しているが、それをさらに確実なものとするために、新たな数値計算を行った。フレーバー数は２の場合を考え、パリティ・フレーバー対称性の自発的破れを調べるために、その対称性を破る秩序変数に結合する外場を導入した数値計算を行い、以下の結果を得た。外場の値がゼロでない場合は、強結合の極限では数値計算の答えと強結合展開による解析的な計算の答えとがよく一致し、格子体積効果もほとんどない[2.3]。この結果は、無限体積では外場をゼロにした極限でも秩序変数がゼロにならない相、つまり、パリティ・フレーバー対称性が自発的に破れる相、が存在することを意味している。と同時にこの場合に強結合展開がいい近似になっていることも示している。強結合極限はゼロ温度の場合に対応しているので、次に温度は低いがゼロでなく有限の場合を調べた。この場合も有限の外場のときの秩序変数の振る舞いは、パリティ・フレーバー対称性が自発的に破れる相の存在を強く示唆している[2.1]。

この２つの結果は、パリティ・フレーバー対称性が自発的に破れる相は温度に関わらず存在することを明らかにした。また、外場をいれる方法が格子ＱＣＤの相構造を調べる場合の有効な方法であることをも示している。

（２）作用を改良した場合の有限温度の相構造

パリティ・フレーバー対称性の破れがゼロ質量のパイ中間子の存在を保証するという機構および有限温度における複雑な相構造は、ウィルソン・フェルミオン作用のようにカイラル対称性をあらわに破る格子作用の場合に普遍的にあてはまると予想される。そのことを確かめるために、ゲージ場の作用として繰り込み群(Renormalization Group)によって改良された作用（以下ではＲＧ作用と呼ぶ）をとり、ウィルソン・フェルミオン作用と組み合わせて有限温度での相構造を調べた。ＲＧ作用は岩崎らによって提唱され、有限の格子間隔によるスケーリングの破れが通常のプラケット作用に比べて小さいことがわかっている作用である。フレーバー数２で外場なしの場合のパイ中間子の質量をＱＣＤ数値計算で調べ、以下のような結果を得た[2.4]。

低温領域では、パイ中間子の質量がゼロになる転移線が２本あることを確認した。この２本にはさまれた領域はパリティ・フレーバー対称性が自発的に破れている相に対応している。また、温度を上げていくとその領域は徐々にせばまっていき、ある有限の温度で２本の線がぶつかり、カスプ構造をなすことも確認した。さらに、有限温度の相転移は２次で転移線はそのカスプの近くを通っていることもわかった。以上の結果は通常のブラケット・ゲージ作用の結果と定性的に同じものであり、ゲージ作用に依らないという相構造の普遍性を示したことになっている。

（３）有限温度の相構造のフレーバー数依存性

フレーバー数が２のウィルソン・フェルミオン作用の場合に発見されたパリティ・フレーバー対称性の破れとその有限温度の相構造は、パイ中間子の質量がゼロになる限り、２以外のフレーバー数の場合にも成り立っているはずである。このことを確かめるためにフレーバー数が３、４の場合のＱＣＤの数値計算を行い、以下の結果を得た[2-1,2-3]。

どちらのフレーバー数の場合のも、低温ではパリティ・フレーバーが自発的に破れる相に対応する領域が存在し、温度を上げるとその２本の境界線が交わりカスプ構造を成すこと、を示した。さらに、フレーバー数が３の場合は、有限温度の相転移線はカスプの近くを通り、カスプの近傍では１次転移であることもわかった。これは、カスプの近傍で有限温度のカイラル相転移が記述できること、また、フレーバー数が２の場合には２次転移であり３の場合は１次転移であるという連続理論での予想とよく対応していること、をも示している。ところが、４フレーバーの場合は、確かに有限温度の相転移線はカスプの近くを通るが、強い１次転移がカスプに近づくにつれ弱くなり、カスプの近傍では１次転移の証拠を見つけることはできなかった。連続理論では４フレーバーの時は１次転移と予想されているので、それに対応する１次転移をカスプの近傍で見つけることは今後の課題である。

（４）有限温度相転移の連続極限

ウィルソン・フェルミオン作用の場合、有限温度のカイラル相転移はカスプの近傍で定義されると思われる。なぜなら、そこではパイ中間子がゼロ質量になり、その近くを有限温度の相転移線が通っているからで、カイラルな有限温度の相転移と考えることができるからである。格子理論の場合は格子間隔が有限であることに付随する系統誤差があるが、それを取り除くためには連続極限をとる必要がある。有限温度の数値計算で連続極限をとるためには、時間方向の格子点数N_Tを、それが空間方向の格子点数より少ないという条件を保ったまま、増やして行かなくてはならない。ウィルソン・フェルミオン作用の有限温度の場合はN_Tを増やしたときにカスプの現れる位置がより弱結合側に移動するはずである。そしてその移動の速さがはやいほど連続極限にはやく近づくことになる。このことを調べるために$N_T=4,8$の数値計算をフレーバー数が２と４の時に行った。どちらのフレーバー数の場合も、$N_T=8$のカスプは４の時のカスプよりも弱結合側に現れることを確認したが、その移動の速さは予想ほどにはやくなかった。ゲージ作用の改良でこの点がどのように改善されるかを研究するのは今後の課題である。

（５）クエンチ近似の相構造

ウィルソン・フェルミオンの相構造をＱＣＤの数値計算で調べるためにはスーパーコンピューターを使っても膨大な計算時間を必要であり、相構造をパラメタ空間のグローバルな領域で調べることは簡単ではない。一方、ＱＣＤの数値計算において、フェルミオンの行列式を１とおいたクエンチ近似を用いると計算時間が大幅に短縮される上に定性的な性質はあまり変わらない。このことに注目して、クエンチ近

似ＱＣＤのグローバルな相構造を研究して、以下の結果を得た[1-1]。

ゼロ温度の場合、弱結合側ではパイ中間子の質量がゼロになる１０本の相転移線とそれに囲まれる５つのパリティ・フレーバーが破れる相が存在することが代表研究者によって予想されていた。今回のクエンチ近似の数値計算の結果、この１０本の相転移線をパイ中間子の質量を測ることで確認した。また、クエンチ近似の有限温度の相転移は１次でありクォークの質量にはよらない。したがって、パイ中間子の質量がゼロになる相転移線が有限温度の効果でカスプをつくった時、１次転移の線がパイ中間子の質量がゼロになる相転移線を横切るか、それともカスプの近傍を通るか、の２つの可能性がある。我々の計算の結果、後者であることがわかり、近似なしの結果と整合している。

（６）２フレーバーＱＣＤのカイラル相転移のスーケーリング解析

有限温度のカイラル相転移の性質を詳しく調べるためには、相転移点の近傍での物理量の振る舞いを調べることが重要である。その時、もし相転移が２次ならば、統計物理学においてよく使われるスケーリング解析が役立つと思われる。我々は、２次転移だと思われる２フレーバーＱＣＤの場合にスケーリング解析を適用し、以下の結果を得た。

連続極限により近いと思われるＲＧゲージ作用とウィルソン・フェルミオン作用の組み合わせの場合は、N_t= 4の場合で既にパラメタの広い範囲でスケーリングが成り立っているように見える。また、このときのスーケーリング指数はO(4)のものと整合していて、平均場近似の指数とは一致していない[2-4]。このことから、ウィルソン・フェルミオン作用のカイラル相転移は２フレーバーの場合には２次転移でO(4)の普遍クラスに属することを強く示唆している。

格子ＱＣＤにおいてはウィルソン・フェルミオン作用とともに、ＫＳフェルミオン作用と呼ばれるものがよく使われている。この作用はカイラル対称性の一部を保つことができるので、有限温度のカイラル相転移の性質を調べるのに適している。ウィルソン・フェルミオン作用とＫＳフェルミオン作用の両者の結果を比較することで、より信頼できる結論を導くことができる。そこで我々はＫＳフェルミオン作用を用いて２フレーバーの場合の相転移のスケーリング解析を行った[1-2,2-2,2-5]。そして、相転移は２次であること、しかしながら、スーケーリング指数は予想されるO(4)やＫＳ作用の対称性であるO(2)の指数のどちらにも近く、どちらか一方であるとは決定できなかった。この点を明らかにするのが今後の課題である。

以上の結果のうち、ウィルソン・フェルミオン作用のパリティ・フレーバー対称性の破れと有限温度の相構造については、研究代表者が国際会議においてレビュー講演をし、その内容は報告集に発表された[2-3]。

格子ＱＣＤの数値計算では有限温度の相転移の研究だけでなく他の物理量なども重要である。それらに関する研究の成果についても簡単にふれておく。

５次元のウィルソン・フェルミオン作用を基にカイラル対称に関する性質を良くしたドメインウォール・フェルミオン作用と呼ばれるものがある。これをカイラルゲージ理論に適用し、問題点を指摘した[1-3,1-6]。また、その作用の超対称をもつ理論への応用を議論した[1-5,2-7]。そして、ＱＣＤへ応用したときの摂動的な繰り込みを計算した[1-5,2-6]。

ハドロンの弱電磁相互作用に関するいろいろな行列要素を計算した。K中間子のバグパラメタの計算[1-7,1-8,2-8,2-9,2-13]やB中間子の崩壊定数の計算[1-9,2-10]、K中間子の2つのパイ中間子への崩壊振幅の計算[1-10,2-11]、B中間子のハドロンとレプトンへの崩壊振幅の計算[2-14]などである。また、重いクォークの繰り込み定数の計算なども行った[2-12]。

ハドロンの質量の精密計算も精力的に行った。クエンチ近似の範囲でのほぼ最終結果になるような計算を遂行した[2-15,2-17]。また、近似なしのQCDでのハドロン質量の系統的な計算も現在進行中である[2-16,2-18]。

本研究の研究課題である「格子QCDによる有限温度相転移の研究」は主に以下の研究者との共同研究を含めて行われた。

岩崎　洋一　（筑波大学物理学系　教授）
金谷　和至　（筑波大学物理学系　助教授）
金田　知之　（筑波大学物理学系　大学院生）
櫃　　昌吾　（筑波大学物理学系　大学院生）
宇川　彰　（筑波大学物理学系　教授）
梅村　俊彰　（筑波大学物理学系　大学院生）
吉江　友照　（筑波大学物理学系　助教授）

UTHEP-373
MPI/PhT/97-70
November 1997

One loop calculation in lattice QCD with domain-wall quarks

[1,2]Sinya Aoki and [1]Yusuke Taniguchi
[1]*Institute of Physics, University of Tsukuba, Tsukuba 305, Japan*
[2]*Max-Planck-Institut für Physik, Föringer Ring 6, D-80805 München, Germany*
(September 22, 1998)

Abstract

One loop corrections to the domain-wall quark propagator are calculated in massless QCD. It is shown that no additative counter term to the current quark mass is generated in this theory, and the wave function renormalization factor of the massless quark is explicitly evaluated. We also show that an analysis with a simple mean-field approximation can explain properties of the massless quark in numerical simulations of QCD with domain-wall quarks.

11.15Ha, 11.30Rd, 12.38Bx, 12.38.Gc

I. INTRODUCTION

The formulation of the lattice fermion in QCD with the chiral symmetry is one of the most fascinating problems theoretically and practically. Although both Wilson and Kogut-Susskind (KS) fermion formulations have been popularly used for the lattice QCD simulations, some disadvantages remain in these formulations: In the Wilson fermion formulation the quark mass has additive quantum correction and the chiral limit is reached only by the fine tuning of the mass parameter. As a general rule we have to take continuum limit tuning the mass appropriately in order to simulate massless QCD. In the KS fermion formulation the number of flavors is restricted and the original flavor symmetry is broken explicitly to some residual one.

The domain-wall fermion formulation, which was originally proposed to define lattice chiral gauge theories [1], has been applied to the lattice QCD [2]. This formulation is expected to have great advantage over the previous two formulations: An advantage over the KS fermion is that the number of flavor is not fixed. This is manifest from its definition. The other advantage over the Wilson fermion is that mass renormalization is multiplicative ($m_{\rm eff} = Z_m m_{\rm tree}$). In other words, if a massless mode exists at the tree level it is stable against the quantum correction. This property is not a trivial one, but only an intuitive discussion on it has been given so far [2]. On the other hand, the recent numerical simulation suggests that the stability of the zero mode holds even non-perturbatively [3]. Therefore an analytical understanding of the domain-wall QCD is now needed. The aim of this paper is to confirm the stability of the massless mode by the lattice perturbation theory and to give explicitly the wave function renormalization of the quark field.

This paper is organized as follows. In section 2 we will give basic tools for the perturbative calculation with the domain-wall fermion. It is enough to present only fermion propagator because other Feynman rules of gauge interaction and gauge propagator are exactly identical to that of the ordinary Wilson fermion. In section 3 we calculate one loop corrections to the fermion propagator. Section 4 is the main part of this paper, where we discuss the renormalization of the zero mode or massless quark field. We take the diagonal basis of the mass matrix of the domain-wall fermion and see that the zero mode is stable against the one loop correction. The wave function renormalization factor of the massless quark field is also given explicitly. Section 5 is devoted to the mean field analysis. We show that properties of the zero mode observed in the numerical simulation [3] are well explained in this approximation. In section 6 we give our conclusion and discussion. In appendices some derivations of formulae used in the text are presented.

In this paper we set the lattice spacing $a = 1$ and take the $SU(N_c)$ gauge group with the gauge coupling constant g and the second Casimir $C_2 = \dfrac{N_c^2 - 1}{2N_c}$. We set $N_c = 3$ in the numerical calculations.

II. PERTURBATION THEORY WITH DOMAIN-WALL FERMION

A. Action

We adopt the domain-wall fermion of Shamir type [2] to describe massless quarks. The domain-wall fermion is a variant of the Wilson fermion with sufficiently many flavors and special form of the mass matrix. Although it is also interpreted as a five dimensional Wilson fermion [1], we prefer to treat it as the multi-flavor system [4].

In this point of view only difference from the Wilson fermion action is the fermion bilinear term. If we separate the QCD action for lattice perturbation theory into fermion and gauge parts,

$$S = S_{\text{fermion}} + S_{\text{gauge}} + S_{\text{GF}} + S_{\text{FP}} + S_{\text{measure}}, \tag{1}$$

the lattice gauge action S_{gauge}, the gauge fixing and the FP-ghost term $S_{\text{GF}} + S_{\text{FP}}$, the invariant measure term S_{measure} and the gauge-fermion interaction terms in S_{fermion} are exactly same as those in the ordinary Wilson fermion perturbation theory [5,6] with many flavors.

The domain-wall fermion action S_{fermion} is written as

$$\begin{aligned} S_{\text{fermion}} = & \sum_{n,m} \overline{\psi}_{m,s} \left(\gamma_\mu D_\mu\right)_{m,n} \psi_{n,s} + \overline{\psi}_{m,s} W^{+\,s,t}_{m,n} P_+ \psi_{n,t} + \overline{\psi}_{m,s} W^{-\,s,t}_{m,n} P_- \psi_{n,t} \\ & + m_q \overline{\psi}_{m,s} \left(\delta_{m,n}\delta_{s,N_s}\delta_{t,1} P_+ + \delta_{m,n}\delta_{s,1}\delta_{t,N_s} P_-\right) \psi_{n,t} \end{aligned} \tag{2}$$

where m, n is four dimensional space index, $s, t = 1, \cdots, N_s$ is the flavor index. Here the Dirac operator is given by

$$\left(\gamma_\mu D_\mu\right)_{n,m} = \sum_\mu \frac{1}{2} \gamma_\mu \left(U_{n,\mu}\delta_{n+\hat{\mu},m} - U^\dagger_{m,\mu}\delta_{n-\hat{\mu},m}\right). \tag{3}$$

and mass matrix $W^\pm_{s,t}$ is defined as

$$W^\pm_{n,m;s,t} = \delta_{s\pm1,t}\delta_{n,m} - W_{n,m}\delta_{s,t} \tag{4}$$

where

$$W_{n,m} = (1-M)\delta_{n,m} + \frac{r}{2}\sum_\mu \left(U_{n,\mu}\delta_{n+\hat{\mu},m} + U^\dagger_{m,\mu}\delta_{n-\hat{\mu},m} - 2\delta_{n,m}\right) \tag{5}$$

is a sum of the Dirac mass term and the Wilson term, which contain gauge fields at this stage, and r is the Wilson parameter, which we set $r = -1$. The parameter m_q is the current quarks mass, but in this paper we only treat the massless QCD taking $m_q = 0$. $P_\pm$ is a projection operator defined by

$$P_\pm = \frac{1 \pm \gamma_5}{2} \tag{6}$$

In our domain-wall fermion action (2) we have Dirac mass M besides the current quark mass m_q. Here we have to notice that M is not the physical quark mass but it is rather an unphysical mass of the cutoff order $(1/a)$ like Wilson term. As will be mentioned later M has an important role as a parameter of the theory: choosing a suitable value for M we have a massless fermion mode for the vanishing current quark mass $(m_q = 0)$.

In order to see the massless fermion mode it is more convenient to be in the momentum representation and pull out the bilinear term. The fermion action in the momentum space is written as

$$S_{\text{fermion}} = \int \frac{d^4p}{(2\pi)^4} \overline{\psi}(-p)_s \left[\sum_\mu i\gamma_\mu \sin p_\mu + W^+(p)_{s,t} P_+ + W^-(p)_{s,t} P_- \right] \psi(p)_t + S_{\text{int.}} \tag{7}$$

where the mass matrix has the following form,

$$W^+(p)_{s,t} = \delta_{s+1,t} - W(p)\delta_{s,t} = \begin{pmatrix} -W(p) & 1 & & \\ & -W(p) & \ddots & \\ & & \ddots & 1 \\ & & & -W(p) \end{pmatrix} \tag{8}$$

$$W^-(p)_{s,t} = \delta_{s-1,t} - W(p)\delta_{s,t} = \begin{pmatrix} -W(p) & & & \\ 1 & -W(p) & & \\ & \ddots & \ddots & \\ & & 1 & -W(p) \end{pmatrix} \tag{9}$$

$$W(p) = 1 - M - r\sum_\mu (1 - \cos p_\mu). \tag{10}$$

The gauge interaction term $S_{\text{int.}}$ is identical to that of the Wilson fermion perturbation theory with N_s flavors.

As will be discussed in appendix C, in spite of the presence of the Dirac mass M this fermion system has one massless fermion mode and $N_s - 1$ excited modes with the mass of cut-off order by virtue of this mass matrix form, provided that $|W(p \sim 0)| < 1$ is satisfied by a suitable choice of the Dirac mass M. Here we take the momentum region $p_\mu \sim 0$ to see the zero mode with physical momenta. At the momentum $p_\mu \sim \pi$, where the doubler emerges in the naive fermion formulation, the parameter condition is not satisfied ($|W(p \sim \pi)| > 1$), so that all N_s fermion modes have mass of the cut-off order.

B. Fermion Propagator

In the next section we will calculate the one loop correction to the fermion propagator. In this subsection we set up the lattice Feynman rules for domain-wall fermion with vanishing current quark mass ($m_q = 0$).

As is discussed in the previous subsection, the domain-wall fermion action is almost same as that of the ordinary Wilson fermion's one with N_s flavors. The peculiar feature of the domain-wall fermion is the form of the fermion propagator, which is given by

$$S_{\text{F}}(p)_{s,t} = \left[i\gamma_\mu \bar{p}_\mu + W^+(p)P_+ + W^-(p)P_- \right]^{-1}_{s,t} \tag{11}$$

where $\bar{p}_\mu = \sin(p_\mu)$. The explicit form is written as

$$S_{\rm F}(p)_{s,t} = \left[(-i\gamma_\mu \overline{p}_\mu + W^-)G_R(s,t)P_+ + (-i\gamma_\mu \overline{p}_\mu + W^+)G_L(s,t)P_-\right]_{st} \tag{12}$$

where

$$\begin{aligned} G_R(s,t) &\equiv \left(\frac{1}{\overline{p}^2 + W^+W^-}\right)_{st} \\ &= G^0(s-t) + A_{++}e^{\alpha(s+t)} + A_{+-}e^{\alpha(s-t)} + A_{-+}e^{\alpha(-s+t)} + A_{--}e^{\alpha(-s-t)} \end{aligned} \tag{13}$$

$$G^0(s-t) = A\left(e^{\alpha(N_s-|s-t|)} + e^{-\alpha(N_s-|s-t|)}\right) \tag{14}$$

$$\begin{pmatrix} A_{++} \\ A_{-+} \end{pmatrix} = \frac{A}{e^{\alpha N_s}(1-We^{\alpha}) - e^{-\alpha N_s}(1-We^{-\alpha})} \begin{pmatrix} (1-We^{-\alpha})(e^{-2\alpha N_s}-1) \\ W(e^{\alpha}-e^{-\alpha}) \end{pmatrix} \tag{15}$$

$$\begin{pmatrix} A_{+-} \\ A_{--} \end{pmatrix} = \frac{A}{e^{\alpha N_s}(1-We^{\alpha}) - e^{-\alpha N_s}(1-We^{-\alpha})} \begin{pmatrix} W(e^{\alpha}-e^{-\alpha}) \\ (1-We^{\alpha})(1-e^{2\alpha N_s}) \end{pmatrix} \tag{16}$$

and

$$\begin{aligned} G_L(s,t) &\equiv \left(\frac{1}{\overline{p}^2 + W^-W^+}\right)_{st} \\ &= G^0(s-t) + B_{++}e^{\alpha(s+t)} + B_{+-}e^{\alpha(s-t)} + B_{-+}e^{\alpha(-s+t)} + B_{--}e^{\alpha(-s-t)} \end{aligned} \tag{17}$$

$$\begin{pmatrix} B_{++} \\ B_{-+} \end{pmatrix} = \frac{A}{e^{\alpha N_s}(1-We^{\alpha}) - e^{-\alpha N_s}(1-We^{-\alpha})} \begin{pmatrix} e^{-\alpha}(e^{-\alpha}-W)(e^{-2\alpha N_s}-1) \\ W(e^{\alpha}-e^{-\alpha}) \end{pmatrix} \tag{18}$$

$$\begin{pmatrix} B_{+-} \\ B_{--} \end{pmatrix} = \frac{A}{e^{\alpha N_s}(1-We^{\alpha}) - e^{-\alpha N_s}(1-We^{-\alpha})} \begin{pmatrix} W(e^{\alpha}-e^{-\alpha}) \\ e^{\alpha}(e^{\alpha}-W)(1-e^{2\alpha N_s}) \end{pmatrix}. \tag{19}$$

Here α and A are defined as

$$\cosh\alpha \equiv \frac{1+W^2+\overline{p}^2}{2W(p)} \tag{20}$$

$$\sinh\alpha = \frac{1}{2W}\sqrt{(1-W^2)^2 + 2(1+W^2)\sum \sin^2 p_\mu + (\sum \sin^2 p_\mu)^2} \tag{21}$$

$$A \equiv \frac{1}{2W\sinh\alpha}\frac{1}{2\sinh(\alpha N_s)} \tag{22}$$

Note that the argument p of W and α is suppressed throughout this paper unless necessary. Since this fermion propagator is invariant under $\alpha \to -\alpha$, we take the $\alpha > 0$ without loss of generality. G_R and G_L are also symmetric in (s,t). See appendix B for the derivation. In the one-loop calculation we use the above propagator in the $N_s \to \infty$ limit.

III. ONE LOOP CALCULATION

A. Diagrams

In this section we calculate the one loop correction to the fermion propagator, which is given by two contributions $\Sigma^{\rm tadpole}(p) + \Sigma^{\rm half-circle}(p)$, from diagrams in Fig. 1.

The 1PI fermion 2-point vertex function is given by

$$V^{(2)}_{1-\text{loop}}(p)_{s,t} = \left[i\gamma_\mu \sin p_\mu + W^+(p)P_+ + W^-(p)P_- - \Sigma(p) \right]_{s,t} \tag{23}$$

with

$$\Sigma(p) = \Sigma^{\text{tadpole}}(p) + \Sigma^{\text{half-circle}}(p). \tag{24}$$

In order to investigate the massless mode of $\Gamma^{(2)}_{1-\text{loop}}(p)_{s,t}$ in the $p_\mu \to 0$ limit, we need only the first few terms in the p_μ expansion. Since the only dimensionful quantity is the external momentum p_μ in our calculation, the higher order terms in the p_μ expansion are also higher order in a.

B. Contribution from Tadpole Diagram

The contribution from the tadpole diagram is written as

$$\Sigma^{\text{tadpole}} = \frac{1}{2} g^2 C_2 \sum_\mu (i\gamma_\mu \sin p_\mu - r \cos p_\mu) \int_{-\pi}^{\pi} \frac{d^4 l}{(2\pi)^4} \frac{1}{4\sin^2 \frac{l}{2}} \delta_{s,t} \tag{25}$$

$$= g^2 C_2 T \left(\frac{1}{2} i\not{p} + 2 \right) \delta_{s,t} + \mathcal{O}(a) \tag{26}$$

where T is the tadpole loop integral

$$T = \int_{-\pi}^{\pi} \frac{d^4 l}{(2\pi)^4} \frac{1}{4\sin^2 \frac{l}{2}} = 0.154612. \tag{27}$$

The first term in Eq. (26) is finite, and the second term linearly diverges in the limit $a \to 0$. We see that Σ^{tadpole} is diagonal in flavor space, and its effect is to modify the mass parameter $M \to \widetilde{M} = M - 2g^2 C_2 T$.

C. Contribution from Half Circle Diagram

The contribution from the half circle diagram in the Feynman gauge

$$\Sigma^{\text{half-circle}}_{s,t} = \int_{-\pi}^{\pi} \frac{d^4 l}{(2\pi)^4} \sum_\mu (-igT^a) \left\{ \gamma_\mu \cos \frac{1}{2}(l_\mu + p_\mu) - ir \sin \frac{1}{2}(l_\mu + p_\mu) \right\}$$
$$\times S_{\text{F}}(l)_{s,t} \times (-igT^a) \left\{ \gamma_\mu \cos \frac{1}{2}(l_\mu + p_\mu) - ir \sin \frac{1}{2}(l_\mu + p_\mu) \right\} \times \frac{1}{\widetilde{(p-l)^2}} \tag{28}$$

cannot be calculated analytically because of its complicated dependence on the flavor indices s, t in the fermion propagator. Here $\hat{p_\mu}$ is defined as $\hat{p}_\mu = 2\sin(p_\mu/2)$.

It is easily seen that the loop integral of (28) has infra-red divergence. As is in the ordinary lattice perturbation theory the infra-red divergence can be written in an analytic form. To do this we separate $\Sigma^{\text{half-circle}}_{s,t}$ as follows:

$$\Sigma_{s,t}^{\text{half-circle}}(p) = \Sigma_{s,t}^{\text{lat.}}(p) + \Sigma_{s,t}^{\text{cont.}}(p) \tag{29}$$

where

$$\Sigma_{s,t}^{\text{lat.}}(p) = \Sigma_{s,t}^{\text{half-circle}}(p) - \Sigma_{s,t}^{\text{cont.}}(p) \tag{30}$$

and $\Sigma_{s,t}^{\text{cont.}}(p)$ is introduced to extract the infra-red divergence:

$$\Sigma_{s,t}^{\text{cont.}}(p) = 2g^2 C_2 \int \frac{d^4l}{(2\pi)^4} \frac{-i\not{l}(C_+P_+ + C_-P_-)_{s,t}}{l^2(p-l)^2}\theta(\pi^2 - l^2)$$

with $(C_+)_{s,t} = (1-w_0^2)w_0^{s+t-2}$, $(C_-)_{s,t} = (1-w_0^2)w_0^{2N_s-s-t}$, and $w_0 = W(0)$. In order to have zero modes with the physical momentum, w_0 should be in the region $w_0^2 \leq 1$. This leads to the condition of M that $0 \leq M \leq 2$. Since $\Sigma_{s,t}^{\text{lat.}}(p)$ is infra-red finite in $p \to 0$ limit, we can evaluate it in the p expansion:

$$\Sigma_{s,t}^{\text{lat.}}(p) = \Sigma_{s,t}^{\text{lat.}}(0) + p_\mu \frac{\partial \Sigma_{s,t}^{\text{lat.}}}{\partial p_\mu}(0) + O(a). \tag{31}$$

The logarithmically divergent part $\Sigma^{\text{cont.}}(p)$ can be calculated analytically, while a linearly divergent and finite terms (the first and the second terms in eq.(31)) have to be evaluated by numerical integrations of loop momenta. After a little algebra we have

$$\Sigma_{s,t}^{\text{half-circle}} = -\left[i\not{p}\left(I_{s,t}^+P_+ + I_{s,t}^-P_-\right) + M_{s,t}^+P_+ + M_{s,t}^-P_-\right] \tag{32}$$

where $I^\pm$ and $M^\pm$ are given by

$$I_{s,t}^\pm = I_{\log}^\pm(s,t) + I_{\text{finite}}^\pm(s,t) \tag{33}$$

$$I_{\log}^\pm(s,t) = \frac{1}{16\pi^2} g^2 C_2 (C_\pm)_{s,t}\left(\ln(\pi^2) + \frac{1}{2} - \ln p^2\right) \tag{34}$$

$$\begin{aligned} I_{\text{finite}}^+(s,t) = g^2 C_2 \int \frac{d^4l}{(2\pi)^4}\frac{1}{\hat{l}^2}\Bigg[&\frac{1}{8}\sum_\mu\left(\cos l_\mu (W^-G_R + W^+G_L)(s,t) + \sin^2 l_\mu (G_L+G_R)(s,t)\right) \\ &+ \sum_\mu \frac{\sin^2 l_\mu}{4(\hat{l}^2)^2}\Bigg((W^-G_R + W^+G_L)(s,t) + 2(\sum_\nu \cos^2 l_\nu/2 - 2\cos^2 l_\mu/2)G_L(s,t) \\ &+ \sum_\nu \sin^2 l_\nu/2 G_R(s,t)\Bigg)\Bigg] - g^2 C_2 (C_+)_{s,t}\int \frac{d^4l}{(2\pi)^4}\frac{1}{(l^2)^2}\theta(\pi^2-l^2) \end{aligned} \tag{35}$$

$$\begin{aligned} I_{\text{finite}}^-(s,t) = g^2 C_2 \int \frac{d^4l}{(2\pi)^4}\frac{1}{\hat{l}^2}\Bigg[&\frac{1}{8}\sum_\mu\left(\cos l_\mu (W^-G_R + W^+G_L)(s,t) + \sin^2 l_\mu (G_L+G_R)(s,t)\right) \\ &+ \sum_\mu \frac{\sin^2 l_\mu}{4(\hat{l}^2)^2}\Bigg((W^-G_R + W^+G_L)(s,t) + 2(\sum_\nu \cos^2 l_\nu/2 - 2\cos^2 l_\mu/2)G_R(s,t) \\ &+ \sum_\nu \sin^2 l_\nu/2 G_L(s,t)\Bigg)\Bigg] - g^2 C_2 (C_-)_{s,t}\int \frac{d^4l}{(2\pi)^4}\frac{1}{(l^2)^2}\theta(\pi^2-l^2) \end{aligned} \tag{36}$$

$$M_{s,t}^+ = g^2 C_2 \int \frac{d^4l}{(2\pi)^4}\frac{1}{\hat{l}^2}\sum_\mu\Bigg[\cos^2 l_\mu/2 (W^+G_L)(s,t) - \sin^2 l_\mu/2 (W^-G_R)(s,t)$$

$$+\frac{1}{2}\sin^2 l_\mu (G_L+G_R)(s,t)\Big] \tag{37}$$

$$M^-_{s,t} = g^2 C_2 \int \frac{d^4l}{(2\pi)^4}\frac{1}{\hat{l}^2}\sum_\mu \Big[\cos^2 l_\mu/2 (W^- G_R)(s,t) - \sin^2 l_\mu/2 (W^+ G_L)(s,t)$$

$$+\frac{1}{2}\sin^2 l_\mu (G_L+G_R)(s,t)\Big] \tag{38}$$

By the dimensional counting $I^\pm$ has $\ln a^2$ divergence and constant terms in a, and $M^\pm$ has $1/a$ linear divergence when lattice spacing a is introduced explicitly. Although $M^\pm$ may have $\ln a^2$ divergence naively, it is canceled by the algebraic relation

$$(W^+(p=0))_{s,t}(1-M)^t = 0 \tag{39}$$

$$(W^-(p=0))_{s,t}(1-M)^{-t} = 0. \tag{40}$$

The logarithmic divergence $\ln a^2$ in $I^\pm$ is given analytically. As we can see from the form of $(C_+)_{s,t} = (1-w_0^2)w_0^{s+t-2}$, $I^+_{\log}$ is localized in the boundary $(s,t)=(1,1)$. This is because the logarithmic divergence comes from the effect of massless fermion mode which is localized in the boundary. The other one $I^-_{\log}$ is also localized in the other boundary $(s,t)=(N_s,N_s)$.

The finite terms and linearly divergent terms should be calculated by repeating the numerical integration $O(N_s^2)$ times. However, as can be seen in the next section, such huge number of integrations can be avoided for the wave-function renormalization of the quark field. On the other-hand, since the structures of $I^\pm_{\text{finite}}$ and $M_\pm$ are useful to understand the domain-wall QCD more deeply, we will give them in the separated paper.

IV. RENORMALIZATION OF QUARKS FIELD

The result obtained in the previous section is summarized in the following form of the effective action for 2 point function with the scale $p^2=(\mu a)^2$ at 1-loop level:

$$\Gamma^{(2)} = \overline{\psi}(-p)_s \left[i\gamma_\mu p_\mu \left(Z^+P_+ + Z^-P_-\right) + \overline{W}^+P_+ + \overline{W}^-P_-\right]_{s,t}\psi(p)_t \tag{41}$$

where

$$Z^\pm = 1 + g^2C_2(I_{\text{tad}} + I^\pm_{\log} + I^\pm_{\text{finite}}) \tag{42}$$

$$\overline{W}^\pm = W^\pm(0) + g^2C_2(M_{\text{tad}} + M^\pm) \tag{43}$$

with

$$I_{\text{tad}}(s,t) = -\frac{1}{2}T\delta_{s,t} = -0.077306\delta_{s,t} \tag{44}$$

$$M_{\text{tad}}(s,t) = -2T\delta_{s,t} = -0.309224\delta_{s,t}. \tag{45}$$

The expressions for $I^\pm_{\log}$, $I^\pm_{\text{finite}}$ and $M^\pm$ are given in the previous section. In this section we consider the renormalization of zero modes, which is interpolated by the quark field: $q(p) = P_+\psi(p)_1 + P_-\psi(p)_{N_s}$. Here we only present the results and give the detail of derivations in appendix C.

A. Diagonalization of mass matrix and stability of zero modes

For the renormalization of zero modes, it is better to use new basis, $\psi^d(p)$ which diagonalize mass matrices $\overline{W}^{\pm}$. This basis are given by the relation that

$$\psi^d_s(p) = U_{s,t}P_+\psi(p) + V_{s,t}P_-\psi(p), \tag{46}$$

where unitary matrices U and V satisfy

$$\left[U\overline{W}^-\overline{W}^+U^\dagger\right]_{s,t} = M_s^2\delta_{s,t}$$
$$\left[V\overline{W}^+\overline{W}^-V^\dagger\right]_{s,t} = M_s^2\delta_{s,t}.$$

In our notation the mass eigen-value squared M_s^2 is arranged in such a way that $M_{N_s}^2$=0, and we can take U and V real matrices without loss of generality.

We calculate U and V at 1-loop level:

$$U = (1+g^2U_1)U_0, \qquad V = (1+g^2V_1)V_0, \tag{47}$$

where tree level matrices U_0 and V_0 are analytically obtained in the large N_s limit as follows:

$$[U_0]_{s,t} = \begin{cases} (2/N_s)^{1/2}\sin\alpha_s(N_s+1-t) & s\neq N_s \\ (1-w_0^2)^{1/2}w_0^{(t-1)} & s = N_s \end{cases} \tag{48}$$

and $[V_0]_{s,t} = [U_0]_{s,N_s+1-t}$, where $w_0 = 1-\widetilde{M}$ with $\widetilde{M} = M+4(u-1)$. Here $u=1$ for the naive perturbation theory, while $u = 1-g^2C_2T/2$ for the tadpole improved perturbation theory. Hereafter we will call both cases "the tree level" and will not distinguish the two cases unless necessary. If we expand the mass eigen-value squared as $(M^2)_s = (M_0^2)_s + g^2(M_1^2)_s$, the tree level one is related to the phase factor α_s such that $2w_0\cos\alpha_s = 1+w_0^2-(M_0^2)_s$. This phase factor, which also satisfies $\sin\alpha_s N_s = w_0\sin\alpha_s(N_s+1)$, is explicitly given as $\alpha_s = \pi s/N_s$ in the large N_s limit. It is also shown that U_0 and V_0 diagonalize $W^\pm$ itself such that $[V_0W^+U_0^\dagger]_{s,t} = [U_0W^-V_0^\dagger]_{s,t} = (M_0)_s\delta_{s,t}$.

We now consider $\overline{W}^\pm$, which is denoted as $\overline{W}^\pm = W_0^\pm + g^2W_1^\pm$, where $(W_0^\pm)_{s,t} = W^\pm(0) = \delta_{t,s\pm1} - w_0$ and $g^2(W_1^\pm)_{s,t} = g^2C_2(M^\pm+M_{\rm tad})_{s,t} + 4(1-u)\delta_{s,t}$. To diagonalize $\overline{W}^\mp\cdot\overline{W}^\pm$ at 1-loop order, U_1 and V_1 should satisfy

$$\begin{aligned}(U_1)_{s,t}(M_0^2)_t &+ (M_0^2)_s(U_1^\dagger)_{s,t} \\ &+ (U_0W_1^-V_0^\dagger\cdot V_0W_0^+U_0^\dagger)_{s,t} + (U_0W_0^-V_0^\dagger\cdot V_0W_1^+U_0^\dagger)_{s,t} = (M_1^2)_s\delta_{s,t},\end{aligned} \tag{49}$$

$$\begin{aligned}(V_1)_{s,t}(M_0^2)_t &+ (M_0^2)_s(V_1^\dagger)_{s,t} \\ &+ (V_0W_1^+U_0^\dagger\cdot U_0W_0^-V_0^\dagger)_{s,t} + (V_0W_0^+U_0^\dagger\cdot U_0W_1^-V_0^\dagger)_{s,t} = (M_1^2)_s\delta_{s,t}.\end{aligned} \tag{50}$$

Using the fact that $(U_1,V_1)_{s,t} = -(U_1,V_1)_{t,s}$ implied by the unitarity and the reality, and $V_0W_0^+U_0^\dagger$ and $U_0W_0^-V_0^\dagger$ are diagonal, we can easily solve the above equation as

$$(U_1)_{s,t} = \frac{(M_0)_t(\widetilde{W_1})_{t,s} + (M_0)_s(\widetilde{W_1})_{s,t}}{(M_0^2)_s - (M_0^2)_t}$$
$$(V_1)_{s,t} = \frac{(\widetilde{W_1})_{s,t}(M_0)_t + (\widetilde{W_1})_{t,s}(M_0)_s}{(M_0^2)_s - (M_0^2)_t}$$

for $s \neq t$, and

$$(M_1^2)_s = 2(\widetilde{W_1})_{s,s}(M_0)_s, \qquad (U_1)_{s,s} = (V_1)_{s,s} = 0, \tag{51}$$

where $\widetilde{W_1} = V_0 W_1 U_0^\dagger$. The mass eigen-value squared $M_s^2 = (M_0^2)_s + g^2(M_1^2)_s$ obtained above leads to the mass eigen-value M_s itself: $M_s = (M_0)_s + g^2(\widetilde{W_1})_{s,s}$. Note that $M_{N_s} = 0$ since $(M_0)_{N_s} = 0$ and $(\widetilde{W_1})_{N_s,N_s} = 0$ in the large N_s limit as is shown in appendix C. This result explicitly demonstrates the stability of the zero modes against 1-loop corrections in domain-wall QCD. As in the case at the tree level, it is shown that

$$(V\overline{W}^+ U^\dagger)_{s,t} = (U\overline{W}^- V^\dagger)_{s,t} = M_s\delta_{s,t} + O(g^4). \tag{52}$$

B. Wave function renormalization for quark fields

After diagonalization of the mass matrix, the effective action for the zero mode field $\psi^d(p)_{N_s} = \chi_0(p)$ becomes

$$\bar{\chi}_0(-p)\left[i\gamma_\mu p_\mu\left(\widetilde{Z_+}P_+ + \widetilde{Z_-}P_-\right)\right]\chi_0(p) \tag{53}$$

where

$$\widetilde{Z_\pm} = 1 - g^2 C_2\frac{T}{2} + \frac{g^2 C_2}{16\pi^2}\left(\log\pi^2 + \frac{1}{2} - \log(\mu a)^2\right) + g^2(I_\pm^d)_{N_s,N_s} \tag{54}$$

with $I_+^d = C_2(U_0 I_{\text{finite}}^+ U_0^\dagger)$ and $I_-^d = C_2(V_0 I_{\text{finite}}^- V_0^\dagger)$. Since the interpolating quark field $q(p)$ is expressed as $q(p) = (U_{N_s 1}P_+ + V_{N_s,N_s}P_-)\chi_0(p)$, and $\langle\chi_0(p)\bar{\chi}_0(-p)\rangle = \left[\frac{1}{\widetilde{Z_+}}P_+ + \frac{1}{\widetilde{Z_-}}P_-\right]\frac{-i\gamma_\mu p_\mu}{p^2}$, we obtain

$$\langle q(p)\bar{q}(-p)\rangle = \left[\frac{U_{N_s 1}^2}{\widetilde{Z_+}}P_+ + \frac{V_{N_s,N_s}^2}{\widetilde{Z_-}}P_-\right]\frac{-i\gamma_\mu p_\mu}{p^2}. \tag{55}$$

Therefore, the renormalized quark field $Q(p)$, which satisfies $\langle Q(p)\bar{Q}(-p)\rangle = \frac{-i\gamma_\mu p_\mu}{p^2}$, is given by $Q(p) = [(Z_F^+)^{1/2}P_+ + (Z_F^-)^{1/2}P_-]q(p)$ with $Z_F^+ = \frac{\widetilde{Z_+}}{U_{N_s 1}^2}$ and $Z_F^- = \frac{\widetilde{Z_-}}{V_{N_s,N_s}^2}$. Since an explicit evaluation shows that $(I_+^d)_{N_s,N_s} = (I_-^d)_{N_s,N_s} \equiv I^d$, thus $\widetilde{Z_+} = \widetilde{Z_-} \equiv \tilde{Z}$, and $(U_{N_s 1})^2 = (V_{N_s,N_s})^2 = 1 - w_0^2$, we finally obtain $Z_F^+ = Z_F^- \equiv Z_F = \frac{\tilde{Z}}{1 - w_0^2}$ where

$$\tilde{Z} = 1 - g^2 C_2\frac{T}{2} + \frac{g^2}{16\pi^2}C_2(\log\pi^2 + \frac{1}{2} - \log(\mu a)^2) + g^2 I^d. \tag{56}$$

Here one unknown constant I^d is given by

$$I^d = C_2 \int \frac{d^4l}{(2\pi)^4} \left\{ \frac{1}{8\hat{l}^2} \sum_\mu \left[\sin^2 l_\mu (\widetilde{G_R} + \widetilde{G_L}) + 2\cos l_\mu (w_0 - W(l)) \widetilde{G_R} \right] \right.$$
$$+ \sum_\mu \frac{\sin^2 l_\mu}{2(\hat{l}^2)^2} \left[(w_0 - W(l)) \widetilde{G_R} + (\sum_\nu \cos^2 l_\nu/2 - 2\cos^2 l_\mu/2) \widetilde{G_L} + \sum_\nu (\sin^2 l_\nu/2) \widetilde{G_R} \right]$$
$$\left. - \frac{1}{(l^2)^2} \theta(\pi^2 - l^2) \right\} \tag{57}$$

where

$$\widetilde{G_L} = A \left[\tilde{G} - \frac{e^\alpha - W}{e^{-\alpha} - W} \frac{1}{(e^\alpha - w_0)^2} \right]$$
$$\widetilde{G_R} = A \left[\tilde{G} - \frac{1}{(e^\alpha - w_0)^2} \right]$$

with

$$A = \frac{1 - w_0^2}{2W \sinh \alpha}$$
$$\tilde{G} = \frac{\sinh \alpha_0 - \sinh \alpha}{2w_0 \sinh \alpha_0 (\cosh \alpha_0 - \cosh \alpha)}$$

and $e^{-\alpha_0} = w_0$. The numerical value of I^d is given in Table I at several values of $\widetilde{M}$, together with the total 1-loop renormalization factor Z_1 ($\tilde{Z} \equiv 1 + g^2 Z_1$) at $\mu a = 1$ and the ratio of the non-tadpole contribution $(Z_1)_{\rm non-tad} \equiv I^d + \frac{C_2}{16\pi^2}(\log \pi^2 + 0.5) = I^d + 0.02355$ to the total one. Note also that the tadpole contribution gives $Z_{\rm tad} \equiv -C_2 T/2 = -0.1031$. From this table, we see that I^d is small and depends on $\widetilde{M}$ very weakly: The value $I^d = -0.01945$ at $\widetilde{M} = 0.05$ monotonically increases (; decreases in the absolute value) to $I^d = -0.01222$ at $\widetilde{M} = 0.95$. Furthermore the non-tadpole contribution $Z_{\rm non-tad}$ is relatively small: 4% at $\widetilde{M} = 0.05$ and 12% at $\widetilde{M} = 0.95$, so that the tadpole contribution becomes dominant at all $\widetilde{M}$. This justifies the use of the tree-level result with the tad-pole improvement. Since $Z_1 \simeq 0.1$, the one-loop correction to the Z factor is about 10 % at $g^2 \sim 1.0$.

V. MEAN FIELD ANALYSIS AT FINITE N_S

As seen in the previous sections, due to the presence of off-diagonal terms in the extra dimension, analysis of the 1-loop correction to domain-wall quarks becomes too complicated to be easily applied to results of the numerical simulations, which should be performed on finite N_s. In this section we adopt an approximated but simpler method to analyze the effect of 1-loop corrections. We call the method the mean field (MF) analysis since the link variable $U_{n,\mu}$ in the fermion action is simply replaced by the mean field u which is independent on n and μ. After this replacement the fermion propagator can be explicitly calculated and result is identical to the one given in Appendix B with the replacement such that $x \to ux$ and $\cos p_\mu \to u \cos p_\mu$. In perturbation theory this is equivalent to the tree level analysis with the tad-pole improvement, which has been shown in the previous section to give about 90 % of the wave function renormalization factor at 1-loop level.

Since we are interested in the zero mode at $s = 1$, we set $s = t = 1$ in the propagator. In this case the zero mode appears in $B_{--}e^{-2\alpha}$ of G_L, which is given at non-zero m_q by

$$B_{--}e^{-2\alpha} = \frac{(1 - We^{-\alpha})(1 - m_q^2)}{2W \sinh(\alpha) F} \tag{58}$$

where

$$\begin{aligned} F &= We^{\alpha} - 1 + m_q^2(1 - We^{-\alpha}) - 4m_q \cdot W \cdot \sinh(\alpha) e^{-\alpha N_s} \\ &\quad + e^{-2\alpha N_s}(1 - We^{-\alpha} + m_q^2(We^{\alpha} - 1)). \end{aligned} \tag{59}$$

In the small momentum limit, this leads to

$$\lim_{p^2 \to 0} B_{--}e^{-2\alpha} = \frac{Z^{-1}}{p^2 + m_F^2} \times \frac{(1 - w_0^2)^2 + p^2 u w_0^2}{(1 - w_0^2)^2 + p^2 u(1 + w_0^2)} \tag{60}$$

where $Z^{-1} = \dfrac{1 - m_q^2}{Au}$, $m_F^2 = \dfrac{B}{Au}$ and $w_0 = 1 - M + 4(1 - u) = 1 - \widetilde{M}$ with

$$\begin{aligned} A &= \frac{1}{1 - w_0^2}\Big[1 + m_q^2 w_0^2 - w_0(1 - w_0^2)m_q^2 + m_q w_0^{N_s} \\ &\quad \times \{2N_s(1 - w_0^2) - 1 - w_0^2 + 2w_0(1 - w_0^2) - N_s(1 - w_0^2)^2/w_0\} \\ &\quad + w_0^{2N_s}\{w_0^2 + m_q^2 - 2N_s(1 - w_0^2) - w_0(1 - w_0^2) + N_s(1 - w_0^2)^2/w_0\}\Big] \\ B &= (1 - w_0^2)\left[m_q^2 - 2m_q w_0^{N_s} + w_0^{2N_s}\right]. \end{aligned}$$

Since the pole in the second factor is in general larger than the physical pole in the first factor, we neglect the second factor in the latter analysis.

Now we use the above formula to understand the behavior of the zero mode observed in ref. [3]. For the value of u there are several choices. The tadpole diagram alone gives

$$u = 1 - g^2 C_2 T/2 = 1 - 0.10307 g^2 \simeq \exp[-0.10307 g^2],$$

where we may take the bare coupling $2N_c/\beta$ or the renormalized coupling $g^2_{\overline{MS}}(\pi/a)$ for g^2 in the above formula. Alternatively we may also use the "observed" value of u: $u = P^{1/4}$ where P is the average value of the plaquette normalized to unity. We adopt the latter one in our analysis. The configurations in ref. [3] generated at $\beta = 5.7$ and $m_q a = 0.01$ by the dynamical Kogut-Susskind quark action give $P = 0.5772$, which leads to $u = 0.872$. In ref. [3] two remarkable features are found for the zero mode: no zero mode is observed for $N_s = 4$ and the zero mode is observed at $M = 1.7$ but not at $M \leq 1.0$ for $N_s = 10$. To explain these we calculate m_F as a function of M for both $N_s = 4$ and 10 at $m_q = 0$, 0.01, 0.02 ,0.03, and plot the results in Fig.2, where solid lines are for $N_s = 4$ and dashed lines for $N_s = 10$. Four lines for each N_s correspond to m_q =0, 0.01, 0.02, 0.03 from below to above around $M = 1.5$. The result tells us the followings. The allowed range for the light fermion is very narrow for $N_s = 4$ (roughly $1.4 < M < 1.6$). This may be a reason why the light state could not be found in the simulation [3]. Note that the allowed range for the zero mode is $0.512 < M < 2.512$ in the $N_s \to \infty$ limit. Although the allowed range becomes

larger for $N_s = 10$ ($1.1 < M < 1.9$), no light state appears at $M \leq 1.0$, as observed in the simulation. Furthermore the order of the fermion mass m_F is reversed to the order of the current quark mass m_q at $M \leq 1.0$: m_F is largest at $m_q = 0$. The plot also supports the fact that the zero mode is observed at $M = 1.7$ in the simulation.

As seen in the above the behavior of the numerical simulation is understandable by the MF analysis, which can supply useful informations on the tuning of parameters in numerical simulations such as N_s, M or m_q before-hand. For example we may take $N_s = 4$ for the simulations, which reduces the cost of both CPU time and memory a lot, if M is appropriately chosen ($M \simeq 1.5$ for $U = 0.872$).

VI. CONCLUSION AND DISCUSSION

In this paper we calculate one-loop correction to the fermion propagator in the massless lattice QCD formulated via domain-wall fermions. We show that the zero mode is stable against the one-loop correction: no additative counter term to the quark mass is generated in the large N_s limit. This property is very different from and superior to the ordinary Wilson fermion formulation. We explicitly calculate the wave-function renormalization factor for the massless quarks and show that the tadpole contribution becomes dominant at all $\widetilde{M}$. We also adopt the mean-field analysis to this model, demonstrating that it can qualitatively explain data obtained in the numerical simulation [3].

Although our results strongly indicate that the domain-wall QCD can avoid the fine tuning problem of the quark mass, the mechanism which gives the zero mode in this formulation has not been fully understood yet. Since our proof for the stability of the zero mode contains an explicit calculation at 1-loop (: $(\widetilde{W_1})_{Ns,N_s} = 0$), it can not be easily carried over to higher orders. The result of numerical simulation [3] suggests that the zero mode is also stable against the non-perturbative dynamics. There may be a yet unknown symmetry which ensures the existence of zero mode in the large N_s limit. To find such a symmetry will be important for our understanding of the formulation

In this paper only the wave-function renormalization factor is explicitly evaluated. Based on the method developed in this paper, it is possible to calculate more complicated quantities such as renormalization factors for the quark mass, currents and 4-fermi operators, which are necessary to get the continuum physics from numerical simulations. The results of this paper also suggest that the smeared quark operator $q^{\rm smear} = \sum_s (w_0^s P_+ \psi_s + w_0^{N_s - s} P_- \psi_s)$ may give better signals than $q = P_+ \psi_1 + P_- \psi_{N_s}$ does, since it has a larger overlap to zero modes.

After this work has been completed, there appears a new paper [7], in which the stability of the zero mode is generally considered.

ACKNOWLEDGMENTS

We would like to thank Dr. Izubuchi for his valuable comments and discussion. Discussions with Drs. Zenkin, Nagai, Kaneda, and Ishizuka are also helpful and encouraging. This work is supported in part by the Grand-in Aid for Scientific Research (Nos. 08640350, 09246206, 2373) from the Ministry of Education, Science and Culture. Y.T. is a JSPS fellow.

APPENDIX A. ACTION AND FEYNMAN RULES

The gauge part of the action is exactly same as that of the ordinary lattice QCD action [6].

$$S_{\rm gauge} = \sum_n \sum_{(\mu\nu)} -\frac{\beta}{N_s} {\rm Re\ tr}\left(U^\dagger_{n,\mu} U^\dagger_{n+\hat{\nu},\mu} U_{n+\hat{\mu},\nu} U_{n,\mu}\right) \tag{61}$$

$$S_{\rm GF} = \sum_n \frac{1}{2\alpha}\left(\nabla_\mu A^a_\mu(n+\frac{1}{2}\hat{\mu})\right)^2 \tag{62}$$

$$S_{\rm FP} = \sum_{n,\mu} (\overline{c}^a_{n+\hat{\mu}} - \overline{c}^a_n)\left[c^b_{n+\hat{\mu}} E^{-1}_{ba}\left(gA_\mu(n+\frac{1}{2}\hat{\mu})\right) - E^{-1}_{ab}\left(gA_\mu(n+\frac{1}{2}\hat{\mu})\right)c^b_n\right] \tag{63}$$

$$S_{\rm measure} = -\frac{1}{2}\sum_n \sum_\mu {\rm tr\,ln}\left(\frac{1-\cos\left(gA^c_\mu(n+\frac{1}{2}\hat{\mu}){\rm ad}(T^c)\right)}{\left(gA^c_\mu(n+\frac{1}{2}\hat{\mu}){\rm ad}(T^c)\right)^2}\right)_{ab} \tag{64}$$

where g is the coupling of the $SU(N_c)$ gauge, $\beta = 2N_c/g^2$. α is the gauge parameter. The actions $S_{\rm FP}$ and $S_{\rm measure}$ is not needed in our calculation at one loop level.

The momentum representation of gauge part is

$$\begin{aligned} S_{\rm gauge} + S_{\rm GF} = & \frac{1}{2}\int \frac{d^4p}{(2\pi)^4} A^a_\mu(-p)\left[\hat{p}^2\delta_{\mu\nu} - (1-\frac{1}{\alpha})\hat{p}_\mu\hat{p}_\nu\right] A^a_\nu(p) \\ & + \cdots \end{aligned} \tag{65}$$

here $+\cdots$ denotes the gluon self interactions which do not come into play in our calculation.

The fermion-gauge interaction terms in the momentum representation is

$$\begin{aligned} S_{\rm int.} = & \sum_{n=1}^\infty \int \frac{d^4k}{(2\pi)^4}\frac{d^4p}{(2\pi)^4}\frac{d^4l_1}{(2\pi)^4}\cdots\frac{d^4l_n}{(2\pi)^4}(2\pi)^4\delta^4(k+p+l_1+\cdots+l_n) \\ & \times \frac{i^n}{n!} g^n A^{a_1}_\mu(l_1)\cdots A^{a_n}_\mu(l_n)\overline{\psi}(k)_s T^{a_1}\cdots T^{a_n} \\ & \times\left[\frac{\gamma_\mu}{2}\left(e^{\frac{i}{2}(p_\mu-k_\mu)} - (-)^n e^{-\frac{i}{2}(p_\mu-k_\mu)}\right) - \frac{r}{2}\left(e^{\frac{i}{2}(p_\mu-k_\mu)} + (-)^n e^{-\frac{i}{2}(p_\mu-k_\mu)}\right)\right]\psi(p)_s. \end{aligned} \tag{66}$$

The domain-wall fermion propagator is already given by the Eq. (12).

The fermion gluon interaction vertices are given by (66). Although there are infinite number of interactions in the lattice perturbation theory, only two of them are needed for the present purpose. One of them is the fermion interaction vertex with one gluon field, which is given by

$$V_1(k,p;l,a;\mu) = -igT^a\{\gamma_\mu\cos\frac{1}{2}(-k_\mu+p_\mu) - ir\sin\frac{1}{2}(-k_\mu+p_\mu)\}. \tag{67}$$

The other is the vertex with two gluon fields, given by

$$V_2(k,p;l_1,a,l_2,b;\mu) = \frac{1}{2}g^2\frac{1}{2}\{T^a,T^b\}\{i\gamma_\mu\sin\frac{1}{2}(-k_\mu+p_\mu) - r\cos\frac{1}{2}(-k_\mu+p_\mu)\}\delta_{\mu\nu}. \tag{68}$$

The gluon propagator is given by

$$G^{ab}_{\mu\nu}(p) = \frac{1}{\hat{p}^2}\left[\delta_{\mu\nu} - (1-\alpha)\frac{\hat{p}_\mu\hat{p}_\nu}{\hat{p}^2}\right]\delta_{ab}. \tag{69}$$

We set $\alpha = 1$ in this paper.

APPENDIX B. DERIVATION OF FREE FERMION PROPAGATOR

In this appendix we derive the free fermion propagator, used in the text. For the later use in perturbative analyses of this model, non-zero current quark mass m_q for finite N_s is considered. See also Refs. [8,4,9]. We also derive the propagator with Majorana mass terms, which becomes important for the lattice definition of the $N = 1$ supersymmetric model via domain-wall fermions [10,11].

A. Propagator with non-zero m_q

The free fermion propagator has the following form:

$$S_{\rm F}(p)_{s,t} = \left[(-i\gamma_\mu \overline{p}_\mu + W_m^-)G_R(s,t)P_+ + (-i\gamma_\mu \overline{p}_\mu + W_m^+)G_L(s,t)P_-\right]_{st}$$

where

$$G_R(s,t) \equiv \left(\frac{1}{\overline{p}^2 + W_m^+ W_m^-}\right)_{st} \qquad \text{and} \qquad G_L(s,t) \equiv \left(\frac{1}{\overline{p}^2 + W_m^- W_m^+}\right)_{st}$$

with

$$(W_m^+)_{s,t} = (W^+)_{s,t} + m_q \delta_{s,N_s}\delta_{t,1} \qquad \text{and} \qquad (W_m^-)_{s,t} = (W^-)_{s,t} + m_q \delta_{s,1}\delta_{t,N_s} \tag{70}$$

We first consider G_R. The following equation is satisfied for G_R:

$$\sum_t \left[(x + W^+W^-)_{s,t} + m_q(W^+_{s1}\delta_{tN_s} + \delta_{s,N_s}W^-_{1t}) + m_q^2\delta_{s,N_s}\delta_{tN_s}\right] G_R(t,u) = \delta_{su} \tag{71}$$

with $x = \overline{p}^2$. Therefore, except $s = N_s$ or 1, this equation is satisfied by

$$G_R(s,t) = G(s,t) + A_{++}e^{\alpha(s+t)} + A_{+-}e^{\alpha(s-t)} + A_{-+}e^{\alpha(-s+t)} + A_{--}e^{\alpha(-s-t)} \tag{72}$$

where

$$G(s,t) = A\left(e^{\alpha(N_s - |s-t|)} + e^{-\alpha(N_s-|s-t|)}\right) \tag{73}$$

becomes a special solution to the equation $(x + W^+W^-)G_R = 1$, with

$$\begin{aligned} \cosh\alpha &\equiv \frac{1 + W^2 + x}{2W(p)} \\ A &\equiv \frac{1}{2W\sinh\alpha}\frac{1}{2\sinh(\alpha N_s)}, \end{aligned} \tag{74}$$

and other terms are general solutions to the equation $(x + W^+W^-)G_R = 0$. We can fix their coefficients $A_{\pm\pm}$ by a boundary condition at $s = 1$:

$$(x + W^2 + 1)G_R(1,t) - W \cdot G_R(2,t) - W \cdot m_q \cdot G_R(N_s,t) = \delta_{1t}, \tag{75}$$

which is simplified to

$$G_R(0,t) - m_q G_R(N_s,t) = 0, \tag{76}$$

and another boundary condition at $s = N_s$:

$$(x+W^2)G_R(N_s,t) - W\cdot G_R(N_s-1,t) - W\cdot m_q \cdot G_R(1,t) + m_q^2 G_R(N_s,t) = \delta_{N_s,t}, \tag{77}$$

which is reduced to

$$G_R(N_s,t) - W\cdot G_R(N_s+1,t) + W\cdot m_q G_R(1,t) - m_q^2 G_R(N_s,t) = 0. \tag{78}$$

Plugging eq.(72) into eqs.(76) and (78) leads to

$$\begin{pmatrix} 1-m_q e^{\alpha N_s} & 1-m_q e^{-\alpha N_s} \\ e^{\alpha N_s}(1-We^{\alpha}-m_q^2+Wm_q e^{\alpha(1-N_s)}) & e^{-\alpha N_s}(1-We^{-\alpha}-m_q^2+Wm_q e^{\alpha(N_s-1)}) \end{pmatrix} \begin{pmatrix} A_{++} & A_{+-} \\ A_{-+} & A_{--} \end{pmatrix}$$
$$= -A \begin{pmatrix} e^{-\alpha N_s}-m_q & e^{\alpha N_s}-m_q \\ 1-We^{-\alpha}-m_q^2+Wm_q e^{-\alpha(N_s+1)} & (1-We^{\alpha}-m_q^2+Wm_q e^{\alpha(N_s+1)}) \end{pmatrix}. \tag{79}$$

Solving this we obtain

$$\begin{pmatrix} A_{++} \\ A_{-+} \end{pmatrix} = \frac{A}{F} \begin{pmatrix} (e^{-2\alpha N_s}-1)(1-We^{-\alpha})(1-m_q^2) \\ 2W\sinh(\alpha)(1-2m_q\cosh(\alpha N_s)+m_q^2) \end{pmatrix}$$
$$\begin{pmatrix} A_{+-} \\ A_{--} \end{pmatrix} = \frac{A}{F} \begin{pmatrix} 2W\sinh(\alpha)(1-2m_q\cosh(\alpha N_s)+m_q^2) \\ (1-e^{2\alpha N_s})(1-We^{\alpha})(1-m_q^2) \end{pmatrix}$$

where

$$F = e^{\alpha N_s}[1-We^{\alpha}+m_q^2(We^{-\alpha}-1)] + 4Wm_q\sinh(\alpha) + e^{-\alpha N_s}[We^{-\alpha}-1+m_q^2(1-We^{\alpha})]. \tag{80}$$

Similarly, plugging the general solution for G_L

$$G_L(s,t) = G(s,t) + B_{++}e^{\alpha(s+t)} + B_{+-}e^{\alpha(s-t)} + B_{-+}e^{\alpha(-s+t)} + B_{--}e^{\alpha(-s-t)} \tag{81}$$

into the boundary conditions

$$G_L(N_s+1,t) - m_q G_L(1,t) = 0 \tag{82}$$
$$G_L(1,t) - W\cdot G_L(0,t) + W\cdot m_q G_L(N_s,t) - m_q^2 G_L(1,t) = 0, \tag{83}$$

we finally obtain

$$\begin{pmatrix} B_{++} \\ B_{-+} \end{pmatrix} = \frac{A}{F} \begin{pmatrix} (e^{-2\alpha N_s}-1)e^{-\alpha}(e^{-\alpha}-W)(1-m_q^2) \\ 2W\sinh(\alpha)(1-2m_q\cosh(\alpha N_s)+m_q^2) \end{pmatrix}$$
$$\begin{pmatrix} B_{+-} \\ B_{--} \end{pmatrix} = \frac{A}{F} \begin{pmatrix} 2W\sinh(\alpha)(1-2m_q\cosh(\alpha N_s)+m_q^2) \\ (1-e^{2\alpha N_s})e^{\alpha}(e^{\alpha}-W)(1-m_q^2) \end{pmatrix}.$$

B. Propagator with the Majorana mass term at N_s

For an application of the free fermion propagator obtained in the domain-wall model, we consider the model with the Majorana mass term on the anti-boundary at $s = N_s$, which has been proposed for a lattice definition of the $N = 1$ super Yang-Mills theory [10,11]. Here we set $m_q = 0$.

A free fermion action of the model with the Majorana mass m_0 can be written in the momentum space as

$$S = \frac{1}{2}\bar{\Psi}(-p)_s D_{s,t}(p)\Psi(p) \tag{84}$$

where

$$\Psi_s(p) = \left(\, \psi_s(p), \bar{\psi}_s(p) \,\right), \qquad \bar{\Psi}_s(p) = \begin{pmatrix} \bar{\psi}_s(p) \\ \psi_s(p) \end{pmatrix}, \tag{85}$$

and

$$D(p) = T_0(p) + m_0 X = \begin{pmatrix} D_0(p) & 0 \\ 0 & -D_0(-p)^T \end{pmatrix} + m_0\delta^2 P_+ I P_- \tag{86}$$

with $(\delta^2)_{s,t} \equiv \delta_{s,N_s}\delta_{N_s,t}$, and

$$P_+ = \begin{pmatrix} P_+ & 0 \\ 0 & P_- \end{pmatrix}, \quad P_- = \begin{pmatrix} P_- & 0 \\ 0 & P_+ \end{pmatrix}, \qquad I = \begin{pmatrix} 0 & I_2 \\ I_2 & 0 \end{pmatrix} = \begin{pmatrix} 0 & 0 & \sigma_2 & 0 \\ 0 & 0 & 0 & \sigma_2 \\ \sigma_2 & 0 & 0 & 0 \\ 0 & \sigma_2 & 0 & 0 \end{pmatrix}$$

in terms of 8×8 matrices. Here

$$D_0(p) = i\gamma_\mu \overline{p}_\mu + W^+ P_+ + W^- P_-, \tag{87}$$

is an inverse of the massless free fermion propagator in the domain-wall QCD.

By expanding D^{-1} in m_0 and rearranging it we obtain

$$\begin{aligned} D^{-1} &= \sum_{n=0}^{\infty} (-T_0^{-1} m_0 P_+ I P_- \delta^2)^n T_0^{-1} \\ &= \sum_{n=0}^{\infty} (-m_0)^n T_0^{-1} \delta P_+ Z^{n-1} I P_- \delta T_0^{-1} \end{aligned} \tag{88}$$

where $Z = I P_- \delta T_0^{-1} \delta P_+$.

Using $Z^2 = -x(G_R(p)_{N_s,N_s})^2 P_+$ and suming over n, we finally get

$$D^{-1} = T_0^{-1} + \left[-m_0 T_0^{-1}\delta P_+ I P_- \delta T_0^{-1} + m_0^2 T_0^{-1}\delta P_+ Z I P_- \delta T_0^{-1} \right] \times \frac{1}{1 + m_0^2 x (G_R(p)_{N_s,N_s})^2}. \tag{89}$$

Explicitly this formula gives, in terms of 2×2 block notations,

$$
\begin{aligned}
D(p)_{11}^{-1} &= -D(-p)_{22}^{-1} = \langle \psi(p)\bar{\psi}(-p)\rangle \\
&= (-i\gamma_\mu \overline{p}_\mu)[Z_+(p)P_+ + Z_-(p)P_-] + M_+(p)P_+ + M_-P_- \qquad (90)
\end{aligned}
$$

where

$$
\begin{aligned}
Z_+(p)_{s,t} &= G_R(p)_{s,t} - \frac{m_0^2 xG}{1+m_0^2 xG^2} G_R(p)_{s,N_s} G_R(p)_{N_s,t} \\
Z_-(p)_{s,t} &= G_L(p)_{s,t} + \frac{m_0^2 G}{1+m_0^2 xG^2} (W^- G_R(p))_{s,N_s} (G_R(p)W^+)_{N_s,t} \\
M_+(p)_{s,t} &= (W^- G_R(p)_{s,t} - \frac{m_0^2 xG}{1+m_0^2 xG^2} (W^- G_R(p))_{s,N_s} G_R(p)_{N_s,t} \\
M_-(p)_{s,t} &= (W^+ G_L(p)_{s,t} - \frac{m_0^2 xG}{1+m_0^2 xG^2} G_R(p)_{s,N_s} (G_R(p)W^+)_{N_s,t}
\end{aligned}
$$

with $G \equiv G_R(p)_{N_s,N_s}$. Similarly

$$
\begin{aligned}
(D(p)_{12}^{-1})_{s,t} &= \langle \psi(p)_s \psi(-p)_t \rangle \\
&= \frac{m_0}{1+m_0^2 xG^2} \Big[xG_R(p)_{s,N_s} G_R(p)_{N_s,t} I_2 P_- - i\overline{p}_\mu \gamma_\mu G_R(p)_{s,N_s} (G_R(p)W^+)_{N_s,t} I_2 P_+ \\
&\quad + i\overline{p}_\mu \gamma_\mu (W^- G_R(p))_{s,N_s} G_R(p)_{N_s,t} I_2 P_- + (W^- G_R(p))_{s,N_s} (G_R(p)W^+)_{N_s,t} I_2 P_+ \Big] \qquad (91)
\end{aligned}
$$

and

$$
\begin{aligned}
(D(p)_{21}^{-1})_{s,t} &= \langle \bar{\psi}(p)_s \bar{\psi}(-p)_t \rangle \\
&= \frac{m_0}{1+m_0^2 xG^2} \Big[xG_R(p)_{s,N_s} G_R(p)_{N_s,t} I_2 P_+ + i\overline{p}_\mu \gamma_\mu^T G_R(p)_{s,N_s} (G_R(p)W^+)_{N_s,t} I_2 P_- \\
&\quad - i\overline{p}_\mu \gamma_\mu^T (W^- G_R(p))_{s,N_s} G_R(p)_{N_s,t} I_2 P_+ + (W^- G_R(p))_{s,N_s} (G_R(p)W^+)_{N_s,t} I_2 P_- \Big]. \qquad (92)
\end{aligned}
$$

See ref. [11] for an application of this result.

APPENDIX C. PROPERTIES OF DIAGONALIZATION MATRICES

In this appendix we derive several properties of diagonalization matrices, U and V, which are used for the renormalization of quarks fields.

Let us consider the tree level diagonalization of matrices $(W_0^\mp \cdot W_0^\pm)$. To diagonalize $(W_0^\mp \cdot W_0^\pm)$, we have to solve the eigen-value problems $(W_0^\mp \cdot W_0^\pm)_{s,t}\phi_\pm^i(t) = (M_0^2)_i \phi_\pm^i(s)$, then U_0 and V_0 are given by normalized eigenvectors $\phi_\pm$: $(U_0)_{s,t} = \phi_+^s(t)$ and $(V_0)_{s,t} = \phi_-^s(t)$. The two eigen-state equations lead to the same equation

$$
-w_0 \left(\phi_\pm^i(s+1) + \phi_\pm^i(s-1)\right) + \left(1 + w_0^2 - (M_0^2)_i\right) \phi_\pm^i(s) = 0 \qquad (93)
$$

but with different boundary conditions:

$$
-w_0 \phi_+^i(0) + \phi_+(1) = 0, \qquad \phi_+^i(N_s+1) = 0 \qquad (94)
$$

or

$$-w_0\phi^i_-(N_s+1)+\phi_-(N_s)=0, \qquad \phi^i_-(0)=0. \tag{95}$$

Therefore, once $\phi^i_+(s)$ is known, the other is easily obtained through $\phi^i_-(s)=\phi^i_+(N_s+1-s)$. Hereafter we consider $\phi^i_+(s)$ only and drop the suffices + and i.

There are two types of solutions to the eigen-state equation. For $(M_0^2)_i \le (1-w_0)^2$ we have a damping solution $\phi(s)=Ae^{-\alpha s}$ with $\cosh\alpha=\dfrac{1+w_0^2-(M_0^2)_i}{2w_0}$. The first boundary condition leads to $e^{-\alpha}=w_0$. This implies $(M_0^2)=0$, and therefore $\phi(s)$ is nothing but the zero mode solution of the domain-wall QCD. For this solution w_0 should satisfy $w_0^2\le 1$ ($0\le M\le 2$). The other boundary condition can be satisfied in the large N_s limit. The normalization constant becomes $A=(1-w_0^2)^{1/2}$. Note that there are no other damping solutions which satisfy the first boundary condition.

If the eigen-value is in the region $(1-w_0)^2\le(M_0^2)_i\le(1+w_0)^2$, we have an oscillating solution $\phi(s)=Ae^{i\alpha s}+Be^{-i\alpha s}$ with $\cos\alpha=\dfrac{1+w_0^2-(M_0^2)_i}{2w_0}$. The two boundary conditions imply

$$\begin{pmatrix} e^{i\alpha}-w_0 & e^{-i\alpha}-w_0 \\ e^{i\alpha(N_s+1)} & e^{-i\alpha(N_s+1)} \end{pmatrix} \times \begin{pmatrix} A \\ B \end{pmatrix} = 0. \tag{96}$$

The existence of the non-trivial solution requires $w_0\sin\alpha(N_s+1)=\sin\alpha N_s$, which leads to $\phi(s)=-Ae^{i\alpha(N_s+1)}\sin\alpha(N_s+1-s)\equiv A_0\sin\alpha(N_s+1-s)$. Without loss of generality we can take real A_0, and the normalization condition gives $A_0=(2/N_s)^{1/2}(1+O(1/N_s))$. Setting $\alpha=a/N_s$ we reduce the equation for α to $w_0\sin a=\sin a$ in the large N_s limit. The solutions $a=\pi n$ with integer n to this equation is translated to N_s-1 independent solutions: $\alpha=\pi n/N_s$ with $n=1,2,\cdots N_s-1$. (Note that $0\le\alpha_s\le\pi$ since $\sin\alpha_s>0$.) Therefore, all eigen-values and eigen-vectors are now obtained, giving

$$[U_0]_{s,t}=\begin{cases} (2/N_s)^{1/2}\sin\alpha_s(N_s+1-t) & s\ne N_s \\ (1-w_0^2)^{1/2}w_0^{(t-1)} & s=N_s \end{cases}, \tag{97}$$

and $[V_0]_{s,t}=[U_0]_{s,N_s+1-t}$.

Next we prove some properties of U_0 and V_0. It is noted that U_0 and V_0 can also diagonalize $W_0^{\pm}$:

$$\left(V_0W_0^{+}U_0^{\dagger}\right)_{s,t}=\delta_{s,t}f_s \tag{98}$$

where

$$f_s=\begin{cases} w_0\cos\alpha_s(N_s+1)-\cos\alpha_sN_s & s\ne N_s \\ 0 & s=N_s \end{cases}. \tag{99}$$

Using the equation for α_s $(s\ne N_s)$ we can show

$$\begin{aligned} f_s^2 &= w_0^2+1-2w_0\left[\sin\alpha_sN_s\sin\alpha(N_s+1)+\cos\alpha_sN_s\cos\alpha_s(N_s+1)\right] \\ &= w_0^2+1-2w_0\cos\alpha_s=(M_0^2)_s. \end{aligned} \tag{100}$$

This proves $f_s = (M_0)_s$ for all s.

It is also important to note that U_0 (V_0) diagonalizes $I^+_{\log}$ ($I^-_{\log}$) terms, since

$$\begin{aligned}\left(U_0 w_0^{s+t-2} U_0^\dagger\right)_{s,t} &= \delta_{s,t}\delta_{s,N_s}(1-w_0^2)\sum_{s,t} w_0^{2(s+t-2)} + O(1/N_s) \\ &= \delta_{s,t}\delta_{s,N_s}(1-w_0^2)^{-1} + O(1/N_s). \end{aligned} \tag{101}$$

Now let us consider quantities including g^2 contributions. We first show that U and V diagonalize $\overline{W}^\pm$ at this order:

$$\begin{aligned} V\cdot\overline{W}^+\cdot U^\dagger &= (1+g^2V_1)V_0(W_0^+ + g^2W_1^+)U_0^\dagger(1+g^2U_1^\dagger) \\ &= V_0\cdot W_0^+U_0^\dagger + g^2\left\{V_1V_0W_0^+U_0^\dagger + V_0W_0U_0^\dagger U_1^\dagger + \widetilde{W_1}^+\right\} \end{aligned} \tag{102}$$

where the coefficient of the g^2 term is simplified to

$$(V_1)_{s,t}(M_0)_t + (M_0)_s(U_1^\dagger)_{st} + (\widetilde{W_1^+})_{s,t} = (\widetilde{W_1^+})_{s,t}\left(1 + \frac{(M_0^2)_t - (M_0^2)_s}{(M_0^2)_s - (M_0^2)_t}\right) = 0 \tag{103}$$

for $s \neq t$, and becomes $(\widetilde{W_1}^+)_{s,s}$ for $s = t$. Eq.(102) then becomes

$$= \left(M_0 + g^2\widetilde{W_1}^+\right)\mathbf{1}.$$

It is necessary for the stability of the zero mode to show that $(\widetilde{W_1}^+)_{N_s,N_s} = 0$. This can be proven as follows.

$$(\widetilde{W_1}^+)_{N_s,N_s} = (1-w_0^2)\sum_{s,t} w_0^{N_s-s}(W_1^+)_{s,t}w_0^{t-1} \tag{104}$$

where W_1^+ is composed of the sum G_L, G_R, $W_0^+G_L$ and $W_0^-G_R$ but

$$\sum_{s,t} w_0^{N_s-s}G(s,t)w_0^{t-1} = O(N_s w_0^{N_s}) \to 0$$

for all $G = G_L$, G_R, $W_0^+G_L$ and $W_0^-G_R$ in the large N_s limit. Therefore eq.(104) vanishes.

For the wave-function renormalization factor we have to know

$$U_{N_s,1} = V_{N_s,N_s} = (U_0)_{N_s,1} + g^2\sum_{t\neq N_s}(U_1)_{N_s,t}(U_0)_{t,1}.$$

Fortunately, since $(U_0)_{t,1} = (2/N_s)^{1/2}\sin\alpha_t(1-1) = 0$, there is no order g^2 contribution and it becomes $U_{N_s,1} = (1-w_0^2)^{1/2}$.

Finally we would like to evaluate $I^d_\pm$ from $I^\pm_{\text{finite}}$. If we define

$$\langle F(s,t)\rangle_U \equiv \sum_{s,t}(U_0)_{N_s,s}F(s,t)(U_0)_{N_s,t}$$

and

$$\langle F(s,t)\rangle_V \equiv \sum_{s,t}(V_0)_{N_s,s}F(s,t)(V_0)_{N_s,t},$$

we can show

$$\langle e^{-\alpha|s-t|}\rangle_{U,V} = (1-w_0^2)\frac{\sinh\alpha_0 - \sinh\alpha}{2w_0\sinh\alpha_0(\cosh\alpha_0-\cosh\alpha)}$$

with $e^{-\alpha_0} = w_0$,

$$\langle e^{-\alpha(s+t-2)}\rangle_U = \langle e^{-\alpha(2N_s-s-t)}\rangle_V = (1-w_0^2)\frac{e^{2\alpha}}{(e^\alpha - w_0)^2}$$

and

$$\langle e^{-\alpha(s+t-2)}\rangle_V = \langle e^{-\alpha(2N_s-s-t)}\rangle_U = 0.$$

Using these formula we obtain

$$\begin{aligned}\langle G_L(s,t)\rangle_U &= \frac{1-w_0^2}{2W\sinh\alpha}\left[\frac{\sinh\alpha_0-\sinh\alpha}{2w_0\sinh\alpha_0(\cosh\alpha_0-\cosh\alpha)} - \frac{e^\alpha - W}{e^{-\alpha}-W}\frac{1}{(e^\alpha-w_0)^2}\right] \\ &= \langle G_R(s,t)\rangle_V \equiv \widetilde{G_L} \qquad (105)\\ \langle G_R(s,t)\rangle_U &= \frac{1-w_0^2}{2W\sinh\alpha}\left[\frac{\sinh\alpha_0-\sinh\alpha}{2w_0\sinh\alpha_0(\cosh\alpha_0-\cosh\alpha)} - \frac{1}{(e^\alpha-w_0)^2}\right] \\ &= \langle G_L(s,t)\rangle_V \equiv \widetilde{G_R} \qquad (106)\end{aligned}$$

and

$$\langle W_0^+ G_L(s,t)\rangle_{U,V} = \langle W_0^- G_R(s,t)\rangle_{U,V} = (w_0 - W)\widetilde{G_R}.$$

The explicit expression for $I^\pm_{\text{finite}}$ is reduced to the final result in terms of $\tilde{G}_{L/R}$: $I^d_+ = I^d_- \equiv I^d$ where

$$\begin{aligned}I^d = C_2\int\frac{d^4l}{(2\pi)^4}\Bigg\{&\frac{1}{8\hat{l}^2}\sum_\mu\left[\sin^2 l_\mu(\widetilde{G_R}+\widetilde{G_L}) + 2\cos l_\mu(w_0 - W(l))\widetilde{G_R}\right] \\ &+\sum_\mu\frac{\sin^2 l_\mu}{2(\hat{l}^2)^2}\left[(w_0-W(l))\widetilde{G_R} + (\sum_\nu\cos^2 l_\nu/2 - 2\cos^2 l_\mu/2)\widetilde{G_L} + \sum_\nu(\sin^2 l_\nu/2)\widetilde{G_R}\right] \\ &-\frac{1}{(l^2)^2}\theta(\pi^2-l^2)\Bigg\}. \qquad (107)\end{aligned}$$

REFERENCES

[1] D. B. Kaplan, *Phys. Lett.* **B288** (1992) 342.

[2] Y. Shamir, *Nucl. Phys.* **B406** (1993) 90; V. Furman and Y. Shamir, *Nucl. Phys.* **B439** (1995) 54.

[3] T. Blum and A. Soni, *Phys. Rev.* **D56** (1997) 174; hep-lat/9706023 .

[4] R. Narayanan and H. Neuberger, *Phys. Lett.* **B302** (1993) 62.

[5] H. Kawai, R. Nakayama and K. Seo, *Nucl. Phys.* **B189** (1981) 40.

[6] L. H. Karsten and J. Smit, *Nucl. Phys.* **B183** (1981) 103.

[7] H. Neuberger, hep-lat/9710089 .

[8] P. Vranas, hep-lat/9705023 .

[9] S. Aoki and H. Hirose, *Phys. Rev.* **D49** (1994) 2604.

[10] J. Nishimura, *Phys. Lett.* **B406** (1997) 215.

[11] S. Aoki, K. Nagai and S. Zenkin, hep-lat/9705001 .

FIGURES

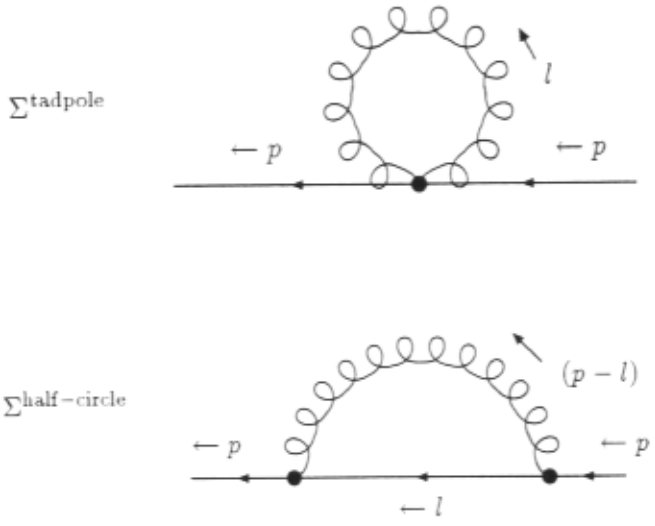

FIG. 1. Diagrams which contribute to the one-loop correction to the fermion propagator. Above: Tadpole diagram. Below: Half-circle diagram.

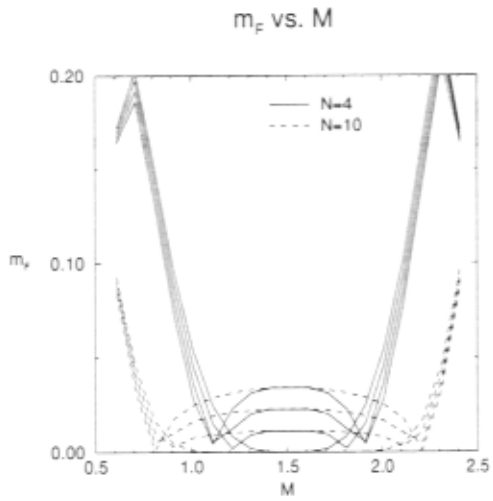

FIG. 2. The fermion mass m_F obtained in the mean-field approximation as a function of M for N_s=4 (solid lines) and N_s=10 (dashed line), at m_q= 0, 0.01, 0.02, 0.03 from below to above around $M = 1.5$.

TABLES

TABLE I. Value of I^d vs $\widetilde{M}$, together with Z_1 and $(Z_1)_{\rm non-tad}/Z_1$

$\widetilde{M}$	I^d	Z_1	$(Z_1)_{\rm non-tad}/Z_1$
0.05	-0.01945(5)	-0.09897	0.041
0.10	-0.01871(5)	-0.09822	0.049
0.15	-0.01804(5)	-0.09756	0.056
0.20	-0.01744(5)	-0.09696	0.063
0.25	-0.01688(5)	-0.09640	0.069
0.30	-0.01636(5)	-0.09589	0.075
0.35	-0.01588(5)	-0.09541	0.080
0.40	-0.01544(5)	-0.09496	0.085
0.45	-0.01502(5)	-0.09454	0.090
0.50	-0.01463(5)	-0.09415	0.095
0.55	-0.01426(5)	-0.09378	0.099
0.60	-0.01392(5)	-0.09345	0.103
0.65	-0.01361(5)	-0.09313	0.107
0.70	-0.01332(5)	-0.09284	0.110
0.75	-0.01305(5)	-0.09257	0.113
0.80	-0.01281(5)	-0.09233	0.116
0.85	-0.01259(5)	-0.09211	0.119
0.90	-0.01239(5)	-0.09191	0.121
0.95	-0.01222(5)	-0.09174	0.124

UTHEP-376
UT-CCP-32
MPI-PhT/97-77
December 1997

The domain-wall model in an asymptotic-free dynamics

S. Aoki [a,b*] and K. Nagai [c†]

[a] *Institute of Physics, University of Tsukuba, Tsukuba, Ibaraki 305, Japan*

[b] *Max-Planck-Institute für Physik, Föhringer Ring 6, D-80805 München, Germany*

[c] *Center for Computational Physics, University of Tsukuba, Tsukuba, Ibaraki 305, Japan*

(September 22, 1998)

Abstract

We investigate a possibility that the rough gauge problem, which have appeared to be a main reason for failures of lattice chiral gauge theories, is cured by an asymptotic-free dynamics. Taking the domain-wall model in 2(+1) dimensions with SU(2) gauge group, we carry out the quenched simulation of gauge fields in the extra dimension. By studying fermion spectra in several volumes, we show that the chiral zero modes exist on the wall without having the spontaneous symmetry breaking thanks to the asymptotic-free dynamics. This result suggests that the rough gauge problem is solved in some class of lattice chiral fermions as well as in 4 dimensions if an asymptotic-free dynamics is incorporated.

11.15Ha, 11.30Rd, 11.90.+t

*aoki@mppmu.mpg.de

†nagai@rccp.tsukuba.ac.jp

I. INTRODUCTION

A definition of lattice chiral gauge theories is one of the long-standing problems in the lattice field theory, in spite of its success as the non-perturbative calculational method for vector gauge theories such as QCD. The difficulty is related to the no-go theorem [1], which proves, under the mild conditions, that it is impossible to define chirally invariant lattice fermion without species doubling. Despite many attempts to put chiral gauge theories on the lattice for many years, so far none of them has been proven to work successfully.

Through analyses of many unsuccessful attempts [2–6], however, a common reason of failures has been recently recognized, called the "rough gauge problem" [6], which we will explain below. A proposed lattice fermion action for one fermion field (in an anomalous representation) necessarily breaks gauge invariance, to reproduce the chiral gauge anomaly in the weak gauge coupling limit, though it may be cancelled by the contribution from other fermion fields. Because of this explicit gauge breaking, the gauge degree of freedom, which varies independently at each site, cannot be gauged away and thus interacts with the fermion, so that the fermion is not a free field even in the weak gauge coupling limit. It is now widely accepted that the roughness of the gauge degree of freedom is an essential reason for failure of the proposals such as the Wilson-Yukawa model [3], the U(1) original domain-wall model [4] and its variant [5], though the detail of the failure depends on the proposal.

By adding the kinetic term for the gauge degree of freedom to the action, one can make it smooth enough to have a desired chiral fermion spectrum. It has been shown in 4 dimensional models that the dynamics of this smoothed gauge degree(= scalar field) simultaneously leads to the condensation of the scalar field, which makes the gauge field massive in lattice unit, so that no chiral gauge theory is defined in the continuum limit. This unsatisfactory correspondence that symmetric phase - vector spectrum or Higgs phase - chiral spectrum seems to be established almost for all models.

Recently, it is, however, claimed that this correspondence is not true and thus the rough gauge problem might be solved if the dynamics of the gauge degree of freedom becomes asymptotic-free [7]. It is actually shown in the spin wave calculation that the rough configuration decouples from the fermion in the overlap formula [8].

In this paper we pursue this possibility further, using the quenched numerical simulation of the original domain-wall model, where the gauge degree of freedom corresponds to the gauge field in the extra dimension. Previously we studied the original domain-wall model with U(1) gauge group both in 2(+1) and 4(+1) dimensions, whose gauge field in the extra dimension has the asymptotic *non*-free dynamics and indeed found no chiral zero mode in the symmetric phase. In contrast, we consider here the SU(2) gauge group in 2(+1) dimensions, where the gauge field in the extra dimension is equivalent to an asymptotic-free SU(2) $\times$ SU(2) non-linear σ model. Therefore there is only one phase, symmetric phase, in the model. By the quenched Monte-Carlo simulation of the model we investigate an existence of chiral zero modes near and below the scaling region of the model. This paper is organized as follows. We explain the original domain-wall model in Sec.II. In Sec.III the method of our analyses is explained, then the results are shown. Our conclusion and discussion are given in Sec.IV.

II. THE DOMAIN-WALL MODEL

The original domain-wall model is the $2k(+1)$-dimensional Wilson fermion whose mass term has a kink-like shape in the extra dimension, vectorically interacting with the $2k(+1)$-dimensional gauge fields. The action of the original model, reformulated in Ref. [9] in terms of a $2k$-dimensional theory, are given as

$$S = S_G + S_F, \tag{1}$$

where S_G is the gauge action and S_F is the fermionic action. S_G is given by

$$S_G = \beta \sum_{n,\mu>\nu} \sum_s \mathrm{ReTr}\left[U^P_{\mu\nu}(n,s)\right] + \beta_s \sum_{n,\mu} \sum_s \mathrm{ReTr}\left[U^P_{\mu D}(n,s)\right], \tag{2}$$

where μ, ν run from 1 to $2k$, n is a $2k$-dimensional lattice point, and s is a coordinate of an extra dimension. $U^P_{\mu\nu}(n,s)$ is a $2k$-dimensional plaquette and $U^P_{\mu D}(n,s)$ is a plaquette containing two link variables in the extra direction ($D = 2k+1$). β is the inverse gauge coupling for the plaquette $U^P_{\mu\nu}$ and β_s is the one for the plaquette $U^P_{\mu D}$. In general, we can take $\beta \neq \beta_s$. The fermionic action S_F on the Euclidean lattice is given by

$$\begin{aligned} S_F = & \frac{1}{2} \sum_{n\mu} \sum_s \bar{\psi}(n,s)\gamma_\mu \left[U_\mu(n,s)\psi(n+\mu,s) - U^\dagger_\mu(n-\mu,s)\psi(n-\mu,s)\right] \\ & + \sum_n \sum_{s,t} \bar{\psi}(n,s)\left[M_0 P_R + M_0^\dagger P_L\right]_{s,t} \psi(n,t) \\ & + \frac{1}{2} \sum_{n\mu} \sum_s \bar{\psi}(n,s)\left[U_\mu(n,s)\psi(n+\mu,s) + U^\dagger_\mu(n-\mu,s)\psi(n-\mu,s) - 2\psi(n,s)\right], \end{aligned} \tag{3}$$

where s, t are an extra coordinates , $P_{R/L} = \frac{1}{2}(1 \pm \gamma_{2k+1})$,

$$\begin{cases} (M_0)_{s,t} = U_D(n,s)\delta_{s+1,t} - a(s)\delta_{s,t} \\ (M_0^\dagger)_{s,t} = U_D^\dagger(n,s-1)\delta_{s-1,t} - a(s)\delta_{s,t}. \end{cases} \tag{4}$$

Here $U_\mu(n,s), U_D(n,s)$ are link variables connecting a site (n,s) to $(n+\mu,s)$ or $(n,s+1)$, respectively. Because of a periodic boundary condition in the extra dimension, s, t run from $-L_s$ to $L_s - 1$, and $a(s)$ is given by

$$\begin{aligned} a(s) &= 1 - m_0 \,\mathrm{sign}\left[(s+\frac{1}{2})\,\mathrm{sign}(L_s - s - \frac{1}{2})\right] \\ &= \begin{cases} 1 - m_0 & (-\frac{1}{2} < s < L_s - \frac{1}{2}) \\ 1 + m_0 & (-L_s - \frac{1}{2} < s < -\frac{1}{2}), \end{cases} \end{aligned} \tag{5}$$

where m_0 is the height of the domain wall mass. It is easy to check that the above fermionic action is identical to the one in $2k(+1)$ dimensions, proposed by Kaplan [2,9]. This model describes chiral fermions for smooth back-ground gauge fields in perturbation theory [10]. We studied the weak coupling limit, where the physical gauge coupling constant $g \to 0$. In this case, all gauge fields in the physical dimensions can be gauged away, while the gauge field in the extra dimension is still dynamical and its dynamics is controlled by β_s. Instead of the gauge degrees of freedom in the edge of the waveguide $(2k+1)$th component of gauge

link variables represent roughness of $2k$-dimensional gauge fields. An important question is whether the chiral zero mode on the domain wall survives in the presence of this rough dynamics.

In this weak coupling limit, the dynamics of the gauge field is equivalent to $2k$-dimensional scalar model with $2L_s$ independent copies where $2L_s$ is the number of sites in the extra dimension, as following way:

$$S_G = \beta_s \sum_s \sum_{n,\mu} \left\{ 1 - \mathrm{ReTr} \left[V(n,s) V^\dagger (n+\mu, s) \right] \right\}, \tag{6}$$

where $V(n,s) = U_D(n,s)$. If the gauge group is SU(N), the above action is equivalent to an SU(N) $\times$ SU(N) non-linear σ model at each s, therefore it is asymptotic-free in 2 dimensions and has only a symmetric phase for all β_s. Larger β_s smoother $V(n,s)$ without having non-zero condensation of $V(n,s)$. We can increase β_s as much as we want till the chiral zero modes will appear on the wall. If it appears at finite β_s we can conclude that the chiral fermion exists in the symmetric phase, so the model passes the first test toward the construction of lattice chiral gauge theories. In this paper we take SU(2) as the gauge group and investigate it in $g \to 0$ limit by the quenched simulation.

III. ANALYSES AND RESULTS

The method of simulation and analysis is essentially the same in Ref. [4] except the gauge group. In order to determine the choices of β_s for the fermion propagator calculation, we first calculate the correlation length of the scalar field $V(n,s)$ and the result is given in Fig. 1 as a function of β_s. Form this figure we estimate that the scaling region, where the correlation length grows exponentially in β_s, begins around $\beta_s = 2.0$. This estimation is consistent with the one estimated from the susceptibility[1] [11]. We also see from the data between $L = 16$ and 32 that the finite size effect in the correlation length is negligible at $\beta_s \leq 2.0$ for $L = 16 \equiv L_{min}$. The relation expected from consistency that $\xi < 8 = L_{min}/2$ also holds at $\beta_s \leq 2$.

From the above result on the correlation length we decide to calculated the fermion propagators at $\beta_s = 1.0$ and 2.0 for several values of m_0 on different sizes of lattices, using a quenched approximation. The fermion mass in the 2-dimensional theory is extracted from the fermion propagator within the $s = 0$ layer as follows[2]. The fermion propagator $G(p)_{st}$ in the 2 dimensional momentum space and the coordinate of the extra dimension is written as

$$G(p)_{s,t} = \left[\left(-i \sum_\mu \gamma_\mu \bar{p}_\mu + M \right) G_R(p) \right]_{s,t} P_L + \left[\left(-i \sum_\mu \gamma_\mu \bar{p}_\mu + M^\dagger \right) G_L(p) \right]_{s,t} P_R. \tag{7}$$

---

[1]Note that the notation of the coupling constant in their study is twice smaller than ours.

[2]The details of this method and the notation are explained in Ref. [4]. However, note that $G_L(G_R)$ here is denoted $G_R(G_L)$ in Ref. [4]

Extracting $G_L(p)_{s=t=0}$ and $G_R(p)_{s=t=0}$ and extrapolate them to $p = 0$ we obtain the (effective) fermion mass m_f as

$$(m_f^L)^2 = \lim_{p\to 0} \frac{1}{G_L(p)_{s=t=0}}$$
$$(m_f^R)^2 = \lim_{p\to 0} \frac{1}{G_R(p)_{s=t=0}} \tag{8}$$

where $L(R)$ for m_f stands for the left-handed(right-handed). We take a periodic boundary condition in the first- and the extra-directions and anti-periodic boundary in the second-direction to avoid possible singularity of a massless fermion. The fermion propagator is obtained from the average over 50 configurations and the errors are estimated by jack-knife method with an unit bin size.

In Fig. 2 the fermion mass extracted in this way is plotted as a function of m_0 at β_s =1.0 and 2.0 on $L \times 32 \times 2L_s$ lattices with L =8, 16, 32 and $L_s = 8$. This figure shows that the right-handed mode becomes massless when m_0 is grater than some critical value: m_0^c. For example, $m_0^c \sim 0.8 - 0.95$ at $\beta_s = 1.0$ and $m_0^c \sim 0.4 - 0.6$ at $\beta_s = 2.0$. On the other hand, the left-handed mode are massive at all m_0. It also shows that the finite size effect is small between $L = 16$ and 32, though some effect is seen, in particular at $\beta = 1.0$, for $L = 8$. This lattice size dependence of fermion masses is consistent with the one of the correlation length of the scalar field, and is very different from the size dependence of the fermion mass for asymptotic non-free cases [4]. These results strongly indicate that the chiral fermion spectrum observed on $L = 16$ and 32 remains in the infinite volume limit: the chiral zero modes exist on the wall in the infinite lattice volume of 2-dimensional physical space-time.

In addition to the analysis on the fermion masses, we carry out the mean-field analysis, which has been shown to be successful to explain not only the existence of the critical value of the domain wall mass, but also the behavior of the fermion propagator [4]. We fit the measured propagator with the form of the mean-field propagator obtained by replacing the link variable to some unknown but constant value z. Note that non-zero value of z means an existence of the chiral zero mode for the range that $1 - z \leq m_0 < 1$. The extracted values of z's are plotted as a function of m_0 in Figs. 3 and 4. Within relatively large errors, z's are always non-zero at both β_s. At $\beta_s = 2$ z depends very weakly on m_0 while it increases as m_0 approaches to 1 at $\beta_s = 1$. A similar m_0 dependence to the latter case has been also seen previously for asymptotic non-free cases [4]. Since z should be constant on m_0 if the mean-field approximation is exact, this m_0 dependence shows the magnitude of the error for the mean-field approximation. Again the finite size effect is small between $L = 16$ and 32, contrary to the case of the asymptotic non-free dynamics [4], and no indication that z goes to zero as volume increases is observed. In conclusion the mean-filed analysis also supports, at least at $\beta_s = 2$, the existence of the chiral zero mode on the wall in the infinite volume limit.

IV. CONCLUSIONS AND DISCUSSIONS

In this paper we numerically investigate an existence of chiral zero modes of the original domain-wall model in the presence of asymptotic-free dynamics in 2(+1) dimensions using

the quenched simulation. The result of the fermion mass on $16 \times 32 \times 16$ and $32 \times 32 \times 16$ suggests that the chiral zero mode observed on the domain-wall at $s = 0$ will survive in the infinite volume limit. The mean-field analysis of the fermion propagator also supports this conclusion.

Although the positive indication is obtained for the construction of lattice chiral gauge theories via the domain-wall model with asymptotic-free dynamics, we have to understand a difference between an asymptotic-free and an asymptotic non-free cases more deeply. It is usually thought that the vacuum expectation value of the scalar field controls the existence of the chiral zero mode in the model: If non-zero the zero mode exists, if not it does not. In terms of the mean field analysis, z is supposed to correspond to the vacuum expectation value. This is a crucial property for the failure of the domain-wall model in the symmetric phase, and this seems true for an asymptotic non-free dynamics [4]. However the result of this paper shows that this does not hold anymore for the asymptotic-free dynamics. Then, what controls the existence of zero modes ? What corresponds to z ? It is likely that some function of the correlation length does it. Since the phase is unique for the SU(2)×SU(2) non-linear σ model in 2 dimensions, the function should be analytic in the correlation length, so that it can vanish only on some points of β_s, but not in the non-zero region of β_s. It is more likely that it vanishes only at $\beta_s = 0$. If this is true the zero mode exists for all β_s except $\beta_s = 0$. However since the scalar field near $\beta_s = 0$ is very rough, the dynamics is very similar to that in the symmetric phase of the asymptotic non-free model. Therefore an existence of zero mode near $\beta_s = 0$ may imply an existence of the zero mode also in the symmetric phase of the asymptotic non-free model. This seems inconsistent with the previous numerical results [4]. The one of solution to this puzzle is perhaps that the allowed range of the domain-wall mass m_0 for the zero mode (: $m_c \leq m_0 \leq 1$) is too narrow to be detected in the numerical simulation at the accuracy of Ref. [4]. This point should be clarified, in order to establish the existence of the chiral zero mode of the asymptotic-free model without doubt.

Since scalar field theories with second derivative terms are asymptotic non-free in 4 dimensions, higher derivative terms have to be introduced to make them asymptotic-free [7]. Since, in terms of gauge fields, these higher derivative terms correspond to the gauge fixing terms, the solution to the rough gauge problem by the asymptotic-free dynamics in 4 dimensions is very similar to the recent proposal to the problem by the gauge fixing for the U(1) theory [12]. The relation between the two should be understood.

If the rough gauge problem of the chiral zero mode in the domain-wall model can indeed be solved by an asymptotic-free dynamics, the rough gauge problems appeared in other models such as the Wilson-Yukawa model and the Waveguide model are also resolved by the same dynamics. Research in this direction is also necessary in order to define lattice chiral gauge theories ultimately.

ACKNOWLEDGEMENTS

Numerical calculations for the present work have been carried out at Center for Computational Physics and on VPP500/30 at Science Information Center, both at University of Tsukuba. This work is supported in part by the Grants-in-Aid of the Ministry of Education (Nos. 08640349, 09246206).

REFERENCES

[1] H. B. Nielsen and M. Ninomiya, Nucl. Phys. **B185**, 20 (1981); erratum: *ibid.* **B195**, 541 (1982); Nucl. Phys. **B193**, 173 (1981); Phys. Lett. **B105**, 219 (1981); L. H. Karsten, Phys. Lett. **B104**, 315 (1981).

[2] D. B. Kaplan, Phys. Lett. **B288**, 342 (1992).
For a recent review of domain-wall model, see, K. Jansen, Phys. Rep. **273** ,1 (1996) .

[3] W. Bock, A. K. De and J. Smit, Nucl. Phys. **B388**, 243 (1992); M. F. L. Golterman, D. N. Petcher and E. Rivas, Nucl. Phys. **B377**, 405 (1992); W. Bock, A. K. De, E. Focht and J. Smit, Nucl. Phys. **B401**, 481 (1993); S. Aoki, H. Hirose and Y. Kikikawa Int. J. Mod. Phys. A**9**, 4129 (1994) .

[4] S. Aoki and K. Nagai, Phys. Rev. **D53**, 5058 (1996); Phys. Rev. **D56**, 1121 (1997).

[5] M. F. L. Golterman, K. Jansen, D. N. Petcher, and J. C. Vink, Phys. Rev. **D49**, 1606 (1994); M. F. L. Golterman and Y. Shamir, Phys. Rev. **D51**, 3026 (1995).

[6] D. N. Petcher, Nucl. Phys. **B** (Proc. Suppl.) **30**, 50 (1993); Y. Shamir, Nucl. Phys. **B** (Proc. Suppl.)**47**, 212 (1996) .

[7] Y. Kikukawa, KUNS-1445, hep-lat/9705024 (In two dimensions); KUNS-1446, hep-lat/9707010 (In four dimensions).

[8] R. Narayanan and H. Neuberger, Nucl. Phys. **B412**, 574 (1994).

[9] R. Narayanan and H. Neuberger, Phys. Lett. **B302**, 62 (1993).

[10] S. Aoki and H. Hirose Phys. Rev. **D49**, 2604 (1994); S. Aoki and R. B. Levien, Phys. Rev. **D51**, 3790 (1995).

[11] Y. Kikukawa and S. Miyazaki, Prog. Theor. Phys. **96**, 1189 (1996).

[12] Y. Shamir, TAUP-2306-95, hep-lat/9512019; Nucl. Phys. **B** (Proc. Suppl.) **53**, 664 (1997); M. Golterman and Y. Shamir, Phys. Lett. **B399**, 148 (1997); W. Bock, M. Golterman and Y. Shamir, TAUP-2447-97, hep-lat/9708019; HU-EP-97-64, hep-lat/9709113; HU-EP-97-65, hep-lat/9709115; TAUP-2454-97, hep-lat/9709154.

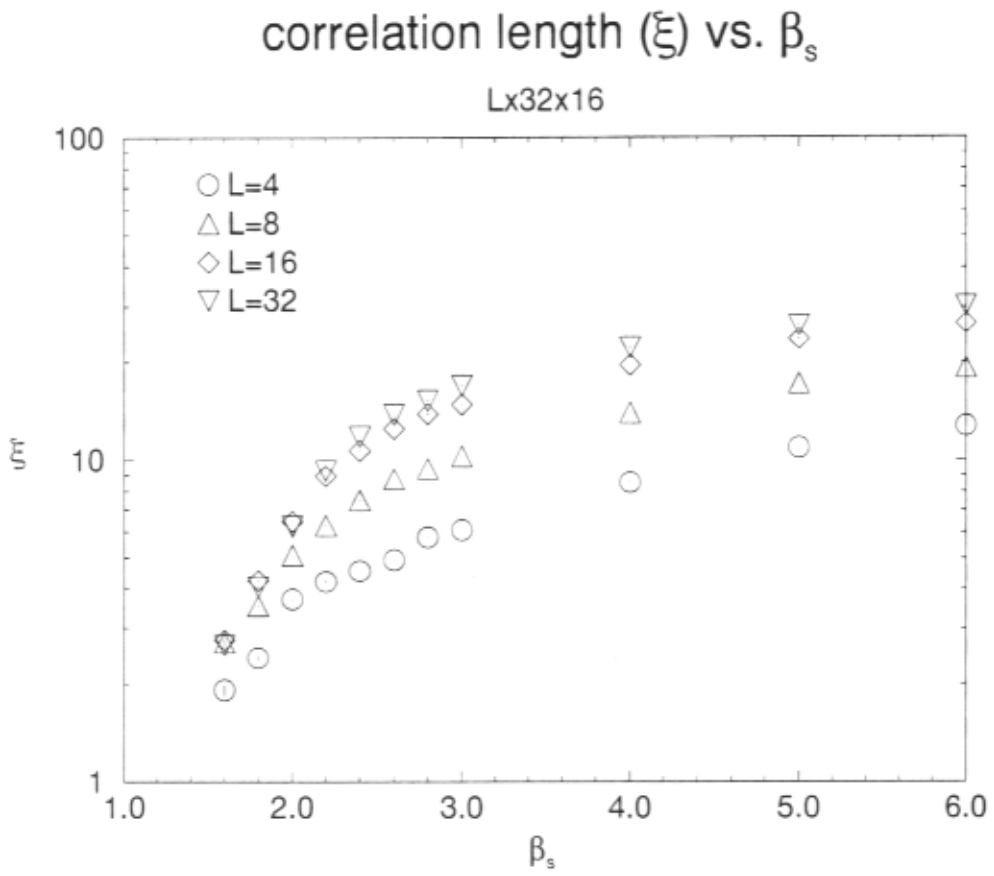

FIG. 1. Correlation length (ξ) vs. β_s on a $L \times 32 \times 16$ lattices with L =4(circles) , 8(up triangles) , 16(diamonds) and 32(down triangles). The error bar is smaller than the symbol.

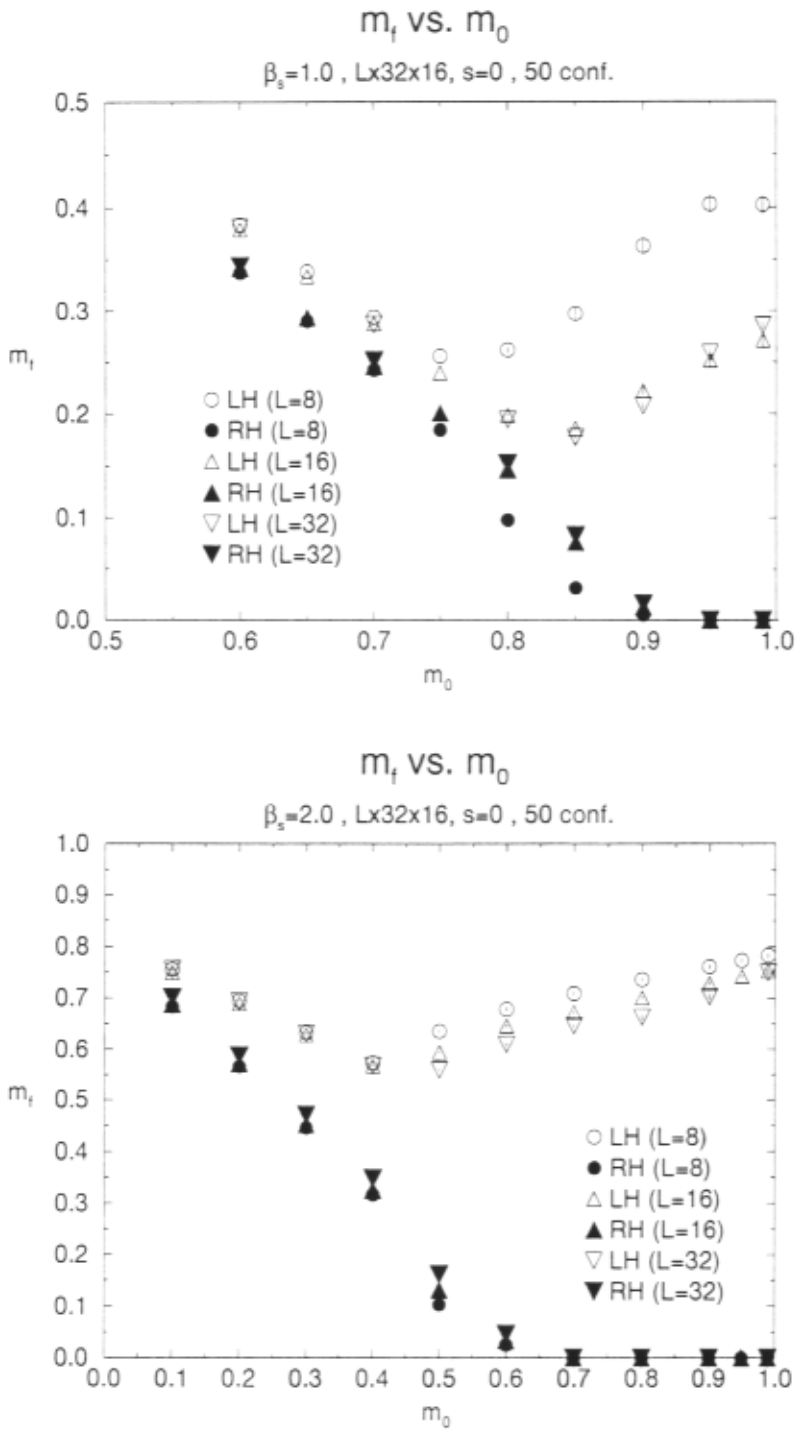

FIG. 2. m_f vs. m_0 at β_s =1.0 and 2.0 on a $L \times 32 \times 16$ lattices with L =8(circles) , 16(up triangles) and 32(down triangles) obtained form the fermion propagator on the domain wall at $s = 0$, for the right-handed fermion (solid symbols) and the left-handed fermion (open symbols).

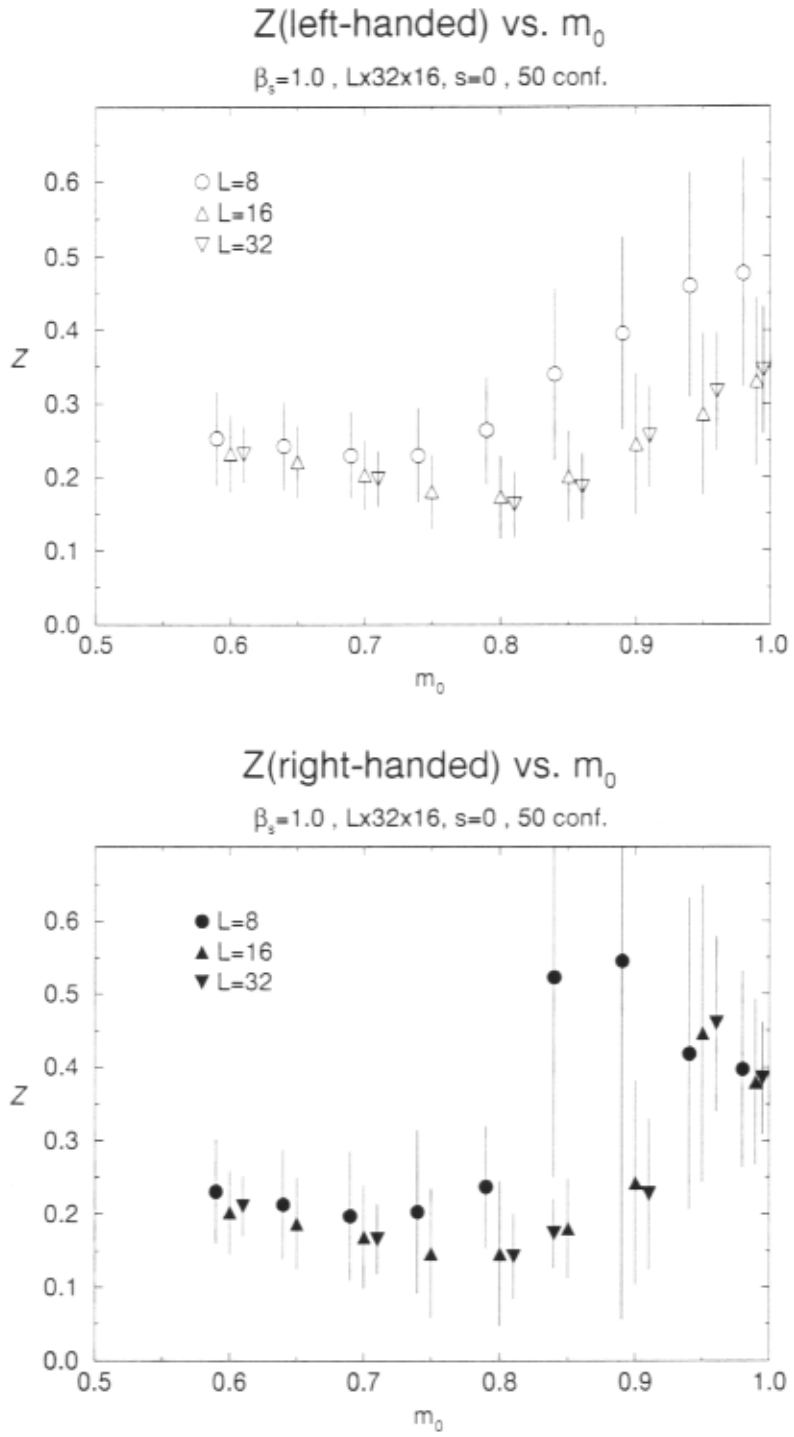

FIG. 3. (a) z(left-handed) vs. m_0 at $\beta_s = 1.0$ (b) z(right-handed) vs. m_0 at $\beta_s = 1.0$ on $L \times 32 \times 16$ lattice with L =8(circles) , 16(up triangles) and 32(down triangles), obtained form the fermion propagator on the domain wall at $s = 0$.

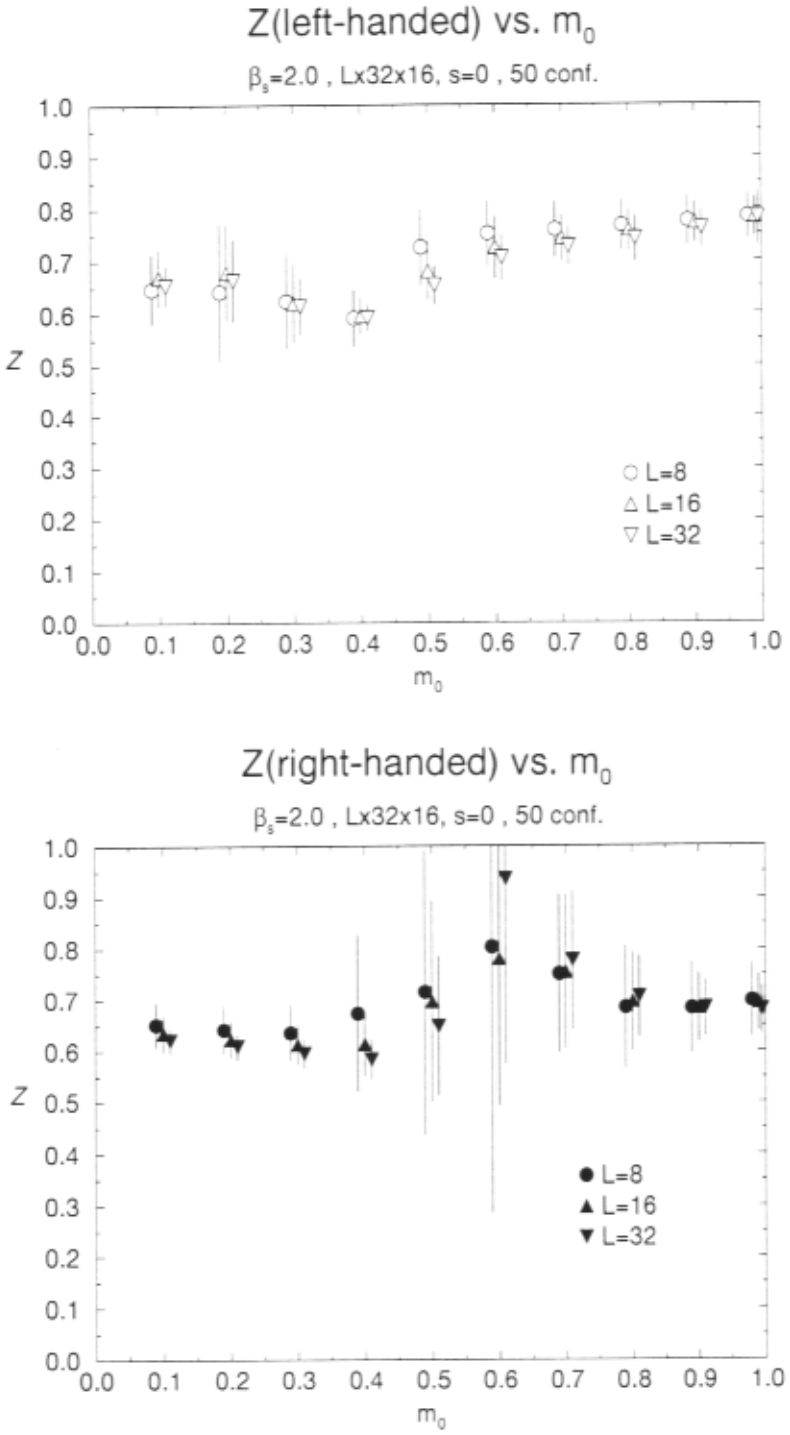

FIG. 4. (a) z(left-handed) vs. m_0 at $\beta_s = 2.0$ (b) z(right-handed) vs. m_0 at $\beta_s = 2.0$ on $L \times 32 \times 16$ lattice with L =8(circles) , 16(up triangles) and 32(down triangles) obtained form the fermion propagator on the domain wall at $s = 0$.

KEK-CP-072
KEK Preprint 97-218
November 1997

$K^+ \to \pi^+\pi^0$ Decay Amplitude with the Wilson Quark Action in Quenched Lattice QCD

JLQCD Collaboration
S. Aoki[a*], M. Fukugita[b], S. Hashimoto[c†], N. Ishizuka[a,d], Y. Iwasaki[a,d], K. Kanaya[a,d], Y. Kuramashi[e], M. Okawa[e], A. Ukawa[a], T. Yoshié[a,d]
[a] *Institute of Physics, University of Tsukuba, Tsukuba, Ibaraki 305, Japan*
[b] *Institute for Cosmic Ray Research, University of Tokyo, Tanashi, Tokyo 188, Japan*
[c] *Computing Research Center, High Energy Accelerator Research Organization (KEK), Tsukuba, Ibaraki 305, Japan*
[d] *Center for Computational Physics, University of Tsukuba, Tsukuba, Ibaraki 305, Japan*
[e] *Institute of Particle and Nuclear Studies, High Energy Accelerator Research Organization (KEK), Tsukuba, Ibaraki 305, Japan*
(September 22, 1998)

Abstract

We present a calculation for the $K^+ \to \pi^+\pi^0$ decay amplitude using a quenched simulation of lattice QCD with the Wilson quark action at $\beta = 6/g^2 = 6.1$. The decay amplitude is extracted from the ratio, the $K \to \pi\pi$ three-point function divided by either K and π meson two-point functions or K meson two-point function and $I = 2$ $\pi\pi$ four-point function; the two different methods yield consistent results. Finite size effects are examined with calculations made on $24^3 \times 64$ and $32^3 \times 64$ lattices, and are shown that they are explained by one-loop effects of chiral perturbation theory. The lattice amplitude is converted to the continuum value by employing a one-loop calculation of chiral perturbation theory, yielding a value in agreement with experiment if extrapolated to the chiral limit. We also report on the K meson B parameter B_K obtained from the $K^+ \to \pi^+\pi^0$ amplitude using chiral perturbation theory.

11.15Ha, 12.38.Gc, 12.38.Aw

*present address: Max-Planck-Institut für Physik, Föhringer Ring 6, D-80805 München, Germany.

†present address: Theoretical Physics Department, Fermi National Accelerator Laboratory, P.O. Box 500, Batavia, IL 60510, USA.

I. INTRODUCTION

Despite the full understanding of the fundamental theory of weak interactions, the non-leptonic decay of hadrons still remains to be the least understood weak process, the most notable problems being $\Delta I = 1/2$ rule and the calculation of ϵ'/ϵ. The predicament originates from the difficulty of evaluating the hadronic matrix element of the product of currents. Much work has already been done to attack this problem using lattice QCD simulations [1–4], but they have not yielded satisfactory results.

Difficulties have proven to be especially severe for the the $\Delta I = 1/2$ amplitudes [1–3]. From the computational point of view the problem lies in a calculation of the so-called eye diagram, which suffers from extremely large statistical fluctuations [1–3,5]. Theoretically, this may be related to mixing of the dimension six weak operator responsible for the decay with operators of lower dimensions whose coefficients diverge linearly in the continuum limit. At a more fundamental level, there is the difficulty [6] that the $K \to \pi\pi$ 3-point function evaluated in Euclidean space-time does not yield information on the phase of the decay amplitude.

Calculation of the $\Delta I = 3/2$ process is known to be easier than that of the $\Delta I = 1/2$ process. For this case mixing of lower dimension operators is absent, and the so-called figure-eight diagrams which represent the $\Delta I = 3/2$ amplitude, have clear signals in numerical simulations. Indeed lattice calculations have been reported by several groups [2,4] quite a long time ago. The problem, however, was that the results turned out to be inconsistent with experiment: lattice calculations have given the amplitude roughly a factor of two larger than experiment.

Two potential origins are suspected to give this discrepancy. One is an issue in the matching of the lattice and continuum operators. Early studies employed the factor $\sqrt{2\kappa}$ for the quark wave function normalization and the bare lattice coupling constant for estimating the renormalization factor of the four-quark weak operator. It is by now well known that the KLM factor $\sqrt{1 - 3\kappa/4\kappa_c}$ [7] and tadpole-improved perturbation theory [8] are more adequate for the operator matching.

Another problem concerns the use of chiral perturbation theory (CHPT) to convert lattice results into the physical amplitude. Only the tree-level formula was known and used in the previous work. The meson mass dependence of lattice calculations appeared consistent with the prediction of the tree-level formula, allowing, however, for large statistical errors. It was probably necessary to use the formula including higher order CHPT effects, but its necessity was not manifest. An interesting development in this connection is a recent calculation of one-loop corrections to the $K^+ \to \pi^+\pi^0$ amplitude in CHPT by Golterman and Leung [9]. Applying their results to the old data obtained by Bernard and Soni [2], they found that one-loop effects decrease the physical amplitude by about 30%.

With the hope to improve the problems posed here, we have carried out a high statistics simulation of the $K^+ \to \pi^+\pi^0$ amplitude in quenched lattice QCD, incorporating various theoretical and technical developments made in recent years. In particular, we discuss in detail how one-loop corrections of CHPT affect physical predictions for the decay amplitude from lattice QCD simulations. We also report on the K meson B parameter B_K obtained from the $K^+ \to \pi^+\pi^0$ amplitude using CHPT.

This paper is organized as follows. After a brief description of simulation parameters in

Sec. II, we explain our method for extracting the decay amplitude in Sec. III. Our results for the $K^+ \to \pi^+\pi^0$ amplitude are presented in Sec. IV with discussion made on one-loop effects of CHPT. Results for B_K are given in Sec. V. Sec. VI summarizes our conclusions.

II. SIMULATION PARAMETERS

Our simulation is carried out in quenched lattice QCD employing the standard plaquette action for gluons at $\beta = 6.1$ and the Wilson action for quarks. We take up, down and strange quarks to be degenerate, and make measurements at four values of the common hopping parameter, $\kappa = 0.1520$, 0.1530, 0.1540, and 0.1543, which correspond to $M_\pi/M_\rho = 0.797$, 0.734, 0.586 and 0.515. In order to examine finite-size effects, simulations are carried out for two lattice sizes, 120 configurations on $24^3 \times 64$ and 65 configurations on $32^3 \times 64$. Gluon configurations are separated by 2000 pseudo heat bath sweeps. Quark propagators are solved with the Dirichlet boundary condition imposed in the time direction and the periodic boundary condition in the space directions.

We adopt $1/a = 2.67(10)$GeV for the physical scale of lattice spacing estimated from the ρ meson mass, and $\kappa_c = 0.15499(2)$ for the critical hopping parameter, which were obtained in our previous study [10]. Our calculations are carried out on the Fujitsu VPP500/80 supercomputer at KEK.

III. METHODS

A. Extraction of decay amplitude

Let us consider the four-quark operator defined by

$$Q_+ = \frac{1}{2} \cdot [\ \bar{s}\gamma_\mu(1-\gamma_5)d\ \bar{u}\gamma_\mu(1-\gamma_5)u + \bar{s}\gamma_\mu(1-\gamma_5)u\ \bar{u}\gamma_\mu(1-\gamma_5)d\ ]\ , \tag{1}$$

which is relevant to $\Delta I = 3/2$ two-pion decay of the K meson. We first discuss our method for extracting the lattice matrix element of the operator Q_+, deferring the question of matching the lattice and continuum operators to Sec. III B.

We extract the decay amplitude from the 4-point correlation function

$$G_Q(t_+, t_0; t; t_K) = \langle 0|W_+(t_+)W_0(t_0)Q_+(t)W_K(t_K)|0\rangle\ . \tag{2}$$

In order to enhance signals we construct wall sources (denoted by W) for all external mesons, and fix gauge configurations to the Coulomb gauge. The wall sources W_K, W_+, and W_0 for K^+, π^+, and π^0 are placed at the time slices t_K, t_+ and t_0 such that $t_K \ll t \ll t_+, t_0$. All mesons are at rest, and the 4-quark operator Q_+ is projected to zero spatial momentum.

In our calculation for temporal lattice size $T = 64$, we place the K meson at $t_K = 4$. The two π mesons are placed at different time slices, $t_+ = 59$ and $t_0 = 60$ to avoid contaminations from Fierz-rearranged terms in the two-pion state that would occur for the choice $t_+ = t_0$.

The correlation function G_Q behaves for $t_K \ll t \ll t_+ \sim t_0$ as

$$
\begin{aligned}
&G_Q(t_+, t_0; t; t_K) \\
&= \langle 0|W_+(0)W_0(t_0 - t_+)|\pi^+\pi^0\rangle \frac{1}{N_{\pi\pi}} \langle \pi^+\pi^0|Q_+(0)|K^+\rangle \frac{1}{N_K} \langle K^+|W_K(0)|0\rangle \\
&\quad \times e^{M_K(t_K - t)} \cdot e^{(t - t_+)M_{\pi\pi}}
\end{aligned} \tag{3}
$$

where N_K denotes the normalization factor of the K meson state, $|\pi^+\pi^0\rangle$ represents the $I = 2$ two-pion state with a mass $M_{\pi\pi}$ and a state normalization factor $N_{\pi\pi}$.

In order to remove the normalization factors in G_Q we calculate the product of the meson 2-point functions given by

$$
G_W(t_+, t_0; t; t_K) = \langle 0|W_0(t_0)\pi^0(t)|0\rangle \langle 0|W_+(t_+)\pi^+(t)|0\rangle \langle 0|K^+(t)W_K(t_K)|0\rangle \ . \tag{4}
$$

Defining a ratio $R_W = G_Q/G_W$, we find

$$
R_W(t_+, t_0; t; t_K) = S_W \cdot \frac{\langle \pi^+\pi^0|Q_+|K^+\rangle}{\langle \pi|\pi|0\rangle^3} \cdot \mathrm{e}^{(t - t_+)\Delta} \tag{5}
$$

where

$$
\Delta = M_{\pi\pi} - 2M_\pi \tag{6}
$$

is a mass shift due to a finite spatial lattice size, and S_W is defined by

$$
S_W = \frac{N_\pi^2}{N_{\pi\pi}} \cdot \frac{\langle 0|W_+(0)W_0(t_0 - t_+)|\pi^+\pi^0\rangle}{\langle 0|W_+(0)|\pi^+\rangle \langle 0|W_0(t_0 - t_+)|\pi^0\rangle} \tag{7}
$$

where $t_0 - t_+ = 1$ in our calculation. The value of S_W should converge to unity for infinite volume.

In Fig. 1 we plot $\langle \pi|\pi|0\rangle^3 \cdot R_W$ at $\kappa = 0.1530$ as a function of time t of the weak operator, where we calculate $\langle \pi|\pi|0\rangle$ from the pion 2-point function for point source and point sink. We observe a clear non-vanishing slope, which means the mass shift Δ being positive. Numerical values of Δ and the decay amplitude $\langle \pi^+\pi^0|Q_+|K^+\rangle$ obtained by a single exponential fit for the time range $t = 18 - 46$ are tabulated in Table I. Here we assume $S_W = 1$, whose justification will be discussed below.

According to Lüscher's formula [11], the finite-size mass shift of the two-pion state is written

$$
\Delta = M_{\pi\pi} - 2M_\pi = -\frac{4\pi a_0}{M_\pi (aL)^3} + O(L^{-4}) \tag{8}
$$

where a_0 is the s-wave scattering length and L is the spatial size. This formula was previously employed to calculate the s-wave $\pi\pi$ scattering length in quenched lattice QCD [12–14]. It was found that lattice calculations give a_0 in good agreement with the prediction of current algebra. Using the current algebra formula $a_0^{I=2} = M_\pi/(8\pi F_\pi^2)$ with $F_\pi = 132$MeV and $1/a = 2.67(10)$GeV, we obtain $a\Delta = 0.015$ for $L = 24$ and 0.006 for $L = 32$. Considering uncertainties arising from terms of $O(L^{-4})$ and the difference between the physical and measured values of F_π, we regard this estimate being consistent with the measured $a\Delta$ (see Table I).

As an alternative method we may remove the normalization factors of the 4-point function G_Q with

$$G_P(t_+, t_0; t; t_K) = \langle 0|W_+(t_+)W_0(t_0)\pi^+(t)\pi^0(t)|0\rangle\langle 0|K^+(t)W_K(t_K)|0\rangle \ . \tag{9}$$

The ratio $R_P = G_Q/G_P$ is independent of t and it does not depend on the wall sources for $t_K \ll t \ll t_+ \sim t_0$,

$$R_P(t_+, t_0; t; t_K) = S_P^{-1} \cdot \frac{\langle \pi^+\pi^0|Q_+|K^+\rangle}{\langle \pi|\pi|0\rangle^3} \tag{10}$$

where

$$S_P = \frac{\langle \pi^+\pi^0|\pi^+\pi^0|0\rangle}{\langle \pi|\pi|0\rangle^2} \tag{11}$$

which should become unity for infinite spatial lattice.

The dependence of R_P on the time t of the weak operator is shown in Fig. 2 for $\kappa = 0.153$, the same hopping parameter as in Fig. 1 for R_W. As expected, a clear plateau is seen for $t \approx 20 - 40$, where effects of excited states near the lattice boundaries already disappear.

In Table I we list $\langle \pi^+\pi^0|Q_+|K^+\rangle$ obtained by fitting R_P to a constant over $t = 22 - 42$ assuming $S_P = 1$. The results from the two methods show good mutual agreement, well within the statistical error of $10 - 15\%$. We note that statistical errors for R_P are smaller, and therefore adopt the matrix elements from R_P to obtain the physical decay amplitude below.

We still have to justify the assumption $S_W = S_P = 1$ used above. This is not *a priori* obvious, especially for S_W, since wall sources are uniformly extended across the spatial lattice, although a good agreement of $\langle \pi^+\pi^0|Q_+|K^+\rangle$ from R_W and R_P implies $S_W \cdot S_P$ close to unity. For S_P chiral perturbation theory predicts a finite-size correction of the form [9],

$$S_P = 1 + \frac{M_\pi^2}{24F_\pi^2(M_\pi aL)^3} \ . \tag{12}$$

This formula indicates that the deviation of S_P from unity would be less than 1% in our simulation. Hence we conclude $S_W \approx 1$.

B. Operator Matching

For the quark field normalization we employ the KLM factor [7]

$$\psi^{continuum} = \sqrt{1 - \frac{3\kappa}{4\kappa_c}}\ \psi^{lattice} \ . \tag{13}$$

Due to CPS symmetry the weak operator Q_+ defined in (1) does not mix with other operators [2]. With the tadpole improvement (with the factor $u_0 = 1/8\kappa_c$) the multiplicative renormalization factor for Q_+, which relates the lattice operator to the continuum one at a scale μ, is given by [15,16]

$$Z(\mu) = 1 + \frac{g^2_{\overline{\rm MS}}(\mu)}{16\pi^2}[-4\log(\mu a/\pi) - 21.140] \tag{14}$$

where the naive dimensional regularization (NDR) is taken with the modified minimum subtraction scheme ($\overline{\rm MS}$) in the continuum.

We employ the $\overline{\rm MS}$ coupling constant estimated as follows. First we obtain g^2_V by [8]

$$-\log P = \frac{1}{3}g^2_V(3.41/a)\{1 - (1.19 + 0.017N_f)\frac{g^2_V(3.41/a)}{4\pi} + O(g^4_V)\} \tag{15}$$

with P the average plaquette. Next we calculate Λ_V from g^2_V using

$$\log(\frac{3.41/a}{\Lambda_V})^2 = \frac{1}{\beta_0 x} + \frac{\beta_1}{\beta_0^2}\log\frac{\beta_1 x/\beta_0}{1 + \beta_1 x/\beta_0} \tag{16}$$

where $\beta_0 = 11 - 2N_f/3$, $\beta_1 = 102 - 38N_f/3$, and $x = g^2_V(3.41/a)/(4\pi)^2$. A perturbative relation $\Lambda_{\overline{\rm MS}} = 0.6252 \cdot \Lambda_V$ then yields $\Lambda_{\overline{\rm MS}}$, with which we can calculate $g^2_{\overline{\rm MS}}(\mu)$ at any scale μ. In the present calculation we find $\Lambda_{\overline{\rm MS}} = 293(11)$MeV with $P = 0.605$ and $1/a = 2.67(10)$GeV at $\beta = 6.1$.

Let A_2 be the physical amplitude for $\Delta I = 3/2$ $K \to \pi\pi$ decay. Experimentally,

$$\sqrt{\frac{3}{2}} \cdot {\rm Re}A_2 \cdot [\frac{G_F}{\sqrt{2}} \cdot V^*_{us}V_{ud}]^{-1} = 10.4 \times 10^{-3} \ \ {\rm GeV}^3 \ . \tag{17}$$

The relation of the decay amplitude to the matrix element of Q_+ is

$$\sqrt{\frac{3}{2}} \cdot {\rm Re}A_2 \cdot [\frac{G_F}{\sqrt{2}} \cdot V^*_{us}V_{ud}]^{-1} = C_+^{(N_f)}(\mu) \cdot \langle \pi^+\pi^0|Q_+^{(N_f)}(\mu)|K^+\rangle \ . \tag{18}$$

On the right-hand side $C_+^{(N_f)}(\mu)$ and $Q_+^{(N_f)}(\mu)$ are the Wilson coefficient function and the renormalized weak operator at a scale μ with superscript N_f the number of quark flavors appropriate for the scale μ. We choose $\mu = 2$GeV to estimate the physical amplitude, and hence $N_f = 4$.

In our calculation, matching of the lattice operator $Q_+^{lattice}$ to the continuum operator $Q_+^{(4)}(2{\rm GeV})$ is not straightforward since the simulation is carried out in quenched QCD ($N_f = 0$). To treat this problem we proceed in the following way. We first match the lattice operator to the continuum operator $Q_+^{(0)}$ for $N_f = 0$ at a scale q^* using the renormalization factor $Z(q^*)$ in (14): $Q_+^{(0)}(q^*) = Z(q^*)Q_+^{lattice}$. The operator $Q_+^{(0)}(\mu)$ at any scale μ can then be obtained by renormalization group evolution in the continuum:

$$\begin{aligned} Q_+^{(0)}(\mu) &= U^{(0)}(\mu, q^*)Q_+^{(0)}(q^*) \\ &= U^{(0)}(\mu, q^*)Z(q^*)Q_+^{lattice} \end{aligned} \tag{19}$$

where $U^{(N_f)}(\mu, \mu')$ is the two-loop renormalization group running factor from scale μ' to μ and it is given by

$$U^{(N_f)}(\mu, \mu') = \Big(\frac{g^2(\mu)}{g^2(\mu')}\Big)^{\frac{\gamma_0}{2\beta_0}}\Big[1 + \frac{g^2(\mu) - g^2(\mu')}{16\pi^2}\Big(\frac{\gamma_1\beta_0 - \gamma_0\beta_1}{2\beta_0^2}\Big)\Big] \ . \tag{20}$$

Here $\gamma_0 = 4$ and $\gamma_1 = -7 + 4N_f/9$ are the one- and two-loop anomalous dimensions for Q_+ [17].

In the spirit of tadpole improvement, the matching point q^* from the lattice to the continuum operator should be chosen to minimize higher order contributions in the renormalization factor $Z(q^*)$. Since an estimate of this value is not available, however, we take $q^* = 1/a$ or π/a and investigate the q^* dependence of the decay amplitude.

We still need to relate the operator $Q_+^{(0)}$ of the $N_f = 0$ theory to the operator $Q_+^{(4)}$ of the $N_f = 4$ theory. Whether such a matching is possible is a problem generally encountered in quenched QCD calculations of weak matrix elements. As a working hypothesis, we assume that there is a scale k^*, typical of the $K^+ \to \pi^+\pi^0$ process, at which the $N_f = 0$ operator matches with the $N_f = 4$ operator,

$$U^{(0)}(k^*, q^*) Q_+^{(0)}(q^*) = Q_+^{(4)}(k^*) \ . \tag{21}$$

We then estimate the decay amplitude for the $N_f = 4$ theory by

$$\begin{aligned} & C_+^{(4)}(\mu) \cdot \langle \pi^+\pi^0 | Q_+^{(4)}(\mu) | K^+ \rangle \\ = \ & C_+^{(4)}(\mu) \cdot U^{(4)}(\mu, k^*) \cdot \langle \pi^+\pi^0 | Q_+^{(4)}(k^*) | K^+ \rangle \\ = \ & C_+^{(4)}(\mu) \cdot D(\mu, k^*, q^*) \cdot \langle \pi^+\pi^0 | Q_+^{lattice} | K^+ \rangle \end{aligned} \tag{22}$$

where

$$D(\mu, k^*, q^*) = U^{(4)}(\mu, k^*) U^{(0)}(k^*, q^*) Z(q^*) \ . \tag{23}$$

For the renormalization group evolution in the continuum we follow Buchalla *et al.* [18]. In particular we use their $C_+^{(4)}(2\text{GeV}) = 0.859$ with $\Lambda_{\overline{\text{MS}}}^{(4)} = 215\text{MeV}$.

The value of the matching scale k^* is not known. The variation of $D(\mu, k^*, q^*)$ with respect to the scale k^*, however, arises from the difference of the Λ parameter and the anomalous dimension of Q_+ for $N_f = 0$ and 4, and so it is expected to be small. The values of $D(\mu, k^*, q^*)$ for several k^* are tabulated for $q^* = 1/a$ and π/a in Table II. We observe that the dependence on k^* is indeed very small, and we set $k^* = 1\text{GeV}$ in the following analysis.

Let us note that the difference of $D(\mu, k^*, q^*)$ for $q^* = 1/a$ and π/a is about 10%. This is the largest systematic error in our operator matching procedure beside the assumption of the matching scale k^*, and it is comparable to our statistical errors.

IV. RESULTS FOR THE $K^+ \to \pi^+\pi^0$ AMPLITUDE

A. Decay amplitude with tree-level CHPT

As in the previous work [2,4] we take degenerate strange and up-down quarks, and assume all external mesons at rest. The amplitude obtained with this kinematics is clearly unphysical, having an energy injection at the weak operator. In order to relate the lattice result to the physical amplitude information is needed on the dependence of the amplitude on the K and π masses away from the physical point.

Earlier calculations have used chiral perturbation theory (CHPT) at tree level for this purpose. The operator Q_+ is decomposed under chiral $\text{SU}(3)_L$ into terms belonging to

$[\mathbf{8}, \Delta I = 1/2]$, $[\mathbf{27}, \Delta I = 1/2]$ and $[\mathbf{27}, \Delta I = 3/2]$. The $[\mathbf{27}, \Delta I = 3/2]$ part of Q_+, which contributes to $K^+ \to \pi^+\pi^0$, is given by

$$\frac{1}{3} \cdot Q_4 = \frac{1}{3} \cdot [2 \cdot Q_+ - \bar{s}\gamma_\mu(1-\gamma_5)d\ \bar{d}\gamma_\mu(1-\gamma_5)d] \ . \tag{24}$$

In general the **27** operator in QCD can be described by operators in CHPT as,

$$\mathcal{O}_{27}^{\rm QCD} = \alpha_{27} \cdot R_{kl}^{ij} \cdot (\Sigma\partial_\mu\Sigma^\dagger)_{ik}(\Sigma\partial_\mu\Sigma^\dagger)_{jl} \tag{25}$$

where, for Q_4, the non-vanishing components of the tensor R_{kl}^{ij} are $R_{31}^{21} = R_{13}^{12} = R_{31}^{12} = R_{31}^{21} = \frac{1}{2}$ and $R_{32}^{22} = R_{23}^{22} = -\frac{1}{2}$, and the pseudoscalar meson field is given by

$$\Sigma = {\rm e}^{i\pi/f} \tag{26}$$

for the full theory, or

$$\Sigma = {\rm e}^{i\pi/f}{\rm e}^{i\eta'/\sqrt{3}f} \tag{27}$$

for the quenched theory. At tree level of CHPT one obtains the formula connecting the physical amplitude and that calculated on the lattice [2] :

$$\langle\pi^+\pi^0|Q_+|K^+\rangle_{phys} = \frac{m_K^2 - m_\pi^2}{2M_\pi^2} \cdot \left(\frac{\alpha_{27}}{\alpha_{27}^q}\right) \cdot \left(\frac{f_q}{f}\right)^3 \cdot \langle\pi^+\pi^0|Q_+|K^+\rangle_{lattice} \tag{28}$$

where $m_K = 497$MeV and $m_\pi = 136$MeV are physical masses, and M_π is the degenerate K and π masses on the lattice. We emphasize that the constant α_{27} and the tree-level decay constant f may take different values in the full and quenched theories. We denote the constants in quenched theory with superscript q.

In Fig. 3 we compare the decay amplitude $C_+ \cdot \langle\pi^+\pi^0|Q_+|K^+\rangle$ of the previous work at $\beta = 5.7$ and 6.0 [2] with ours at $\beta = 6.1$. Here, as a working hypothesis, we set α_{27} and f to be equal in full and quenched theories. For the sake of comparison, our data are analyzed in a manner parallel to that in Ref. [2] as much as possible, *i.e.*, employing the traditional $\sqrt{2\kappa}$ normalization for quark fields, no tadpole improvement in the renormalization factor, and applying the tree-level relation (28). The matching factor (23) with $q^* = \pi/a$ is applied in our results for consistency. Since the normalization adopted in Ref. [2] for comparison with experiment differs from ours, we plot the results divided by the experimental value. In view of various differences in the simulation parameters and details of analysis procedures, the values from the two studies are taken to be consistent, both being larger than experiment roughly by a factor of two.

Let us note that our results, which attain errors of about 10%, show a clear dependence on the lattice meson mass M_π. The presence of finite-size effects is also evident, exhibiting a decrease between 24^3 and 32^3 spatial sizes. We observe that these features were present in the previous simulations when examined in the light of our results, but they were not evident at the time because of large statistical errors of $20 - 30\%$.

In Fig. 4 we show how the use of the KLM normalization affects the meson mass dependence of the decay amplitude (plotted with filled symbols) as compared to the conventional normalization $\sqrt{2\kappa/2\kappa_c}/2$ (open symbols). While the amplitudes for small M_π change only slightly, those for larger M_π increase by about 20%, which is beyond the statistical error by a factor of two. A significant meson mass dependence and finite-size effects observed in our data show that tree-level CHPT is inadequate to extract the physical amplitude from lattice calculations.

B. Decay amplitude with one-loop CHPT

Recently Golterman and Leung have carried out a one-loop calculation of CHPT for the decay amplitude in full and quenched QCD for degenerate and non-degenerate K and π mesons [9]. Their formula also includes finite-size correction terms. Combining with the one-loop formula calculated for the physical point [19], we analyze how our results are changed by one-loop effects of CHPT.

Let us denote by $\langle\pi^+\pi^0|Q_+|K^+\rangle_{phys}$ the physical amplitude in the full theory with non-degenerate K and π mesons of mass m_K and m_π, and by $\langle\pi^+\pi^0|Q_+|K^+\rangle_{lattice}$ the amplitude in the quenched theory with degenerate K and π mesons of mass M_π. According to Golterman and Leung,

$$\langle\pi^+\pi^0|Q_+|K^+\rangle_{phys} = \frac{m_K^2 - m_\pi^2}{2M_\pi^2} \cdot \left(\frac{\alpha_{27}}{\alpha_{27}^q}\right) \cdot \left(\frac{f_q}{f}\right)^3 \cdot Y \cdot \langle\pi^+\pi^0|Q_+|K^+\rangle_{lattice} \tag{29}$$

where α and f are defined in (25–27), and the factor Y is given by

$$Y = \frac{1 + \frac{m_\pi^2}{(4\pi f_\pi)^2}\Big[U + d\Big]}{1 + \frac{M_\pi^2}{(4\pi F_\pi)^2}\Big[-3\log\Big(\frac{M_\pi}{\Lambda^q}\Big)^2 + F(M_\pi aL) + d_q\Big]} \ . \tag{30}$$

The numerator of Y represents the one-loop effect in the full theory, and the denominator is the corresponding effect in the quenched theory. The dimensionless constants d and d_q are the contact term coefficients arising from the $O(p^4)$ terms of the chiral Lagrangian. f_π and F_π are the one-loop corrected decay constants in the full and quenched theories, which differ from the tree-level values f and f_q. In the numerator of Y, U is a complicated function of physical K and π masses, the decay constant f_π and f_K, and the cutoff of CHPT for the full theory Λ^{cont}, and a numerical approximation is

$$U = A + B \cdot \log\Big(\frac{m_\pi}{\Lambda^{cont}}\Big)^2 \tag{31}$$

where $A = -104.73$ and $B = -29.57$ for $m_\pi = 136$MeV, $m_K = 497$MeV, $f_\pi = 132$MeV, and $f_K = 160$MeV. In the denominator of (30), Λ^q is the cutoff of CHPT for quenched QCD, and $F(M_\pi aL)$ represents finite-size corrections for a spatial size L which takes the form

$$F(M_\pi aL) = \frac{17.827}{M_\pi aL} + \frac{12\pi^2}{(M_\pi aL)^3} \ . \tag{32}$$

We set α_{27} and f to be equal in the quenched and full theories as in the analysis with the tree-level CHPT. We initially ignore the effects of $O(p^4)$ terms of the chiral Lagrangian d and d_q. We leave Λ^{cont} and Λ^q to be different, however, and examine the dependence of the results on these cutoffs.

In Fig. 5 we plot the one-loop corrected decay amplitude for $\Lambda^q = 770$MeV and 1GeV for the choice $\Lambda^{cont} = 770$MeV. We set $f_\pi = F_\pi = 132$Mev in (30), and the finite-size corrections $F(M_\pi aL)$ are taken into account. The results of a similar analysis for the choice $\Lambda^{cont} = 1$GeV are plotted in Fig. 6.

An important feature observed in Figs. 5 and 6 is that the size dependence seen with the tree-level analysis in Fig. 4 is removed after finite-size corrections at the one-loop level. At

the same time, the amplitude decreases by $30-40\%$ over the range of meson mass covered in our simulation.

Another noteworthy feature in Figs. 5 and 6 is that a sizable lattice meson mass dependence still remains in the amplitude, and that the magnitude of the slope depends sensitively on the choice of Λ^q. This feature can be understood as arising from the $O(p^4)$ coupling constants in the quenched theory, *i.e.*, d_q in (30), which was ignored above. If we denote our present results by $\langle\pi^+\pi^0|Q_+|K^+\rangle_{ours}$ we find from (30) that

$$\langle\pi^+\pi^0|Q_+|K^+\rangle_{ours} = \langle\pi^+\pi^0|Q_+|K^+\rangle_{phys} \cdot \frac{1+\frac{M_\pi^2}{(4\pi F_\pi)^2}d_q}{1+\frac{m_\pi^2}{(4\pi f_\pi)^2}d} \tag{33}$$

showing the presence of a term linear in M_π^2. We note furthermore that d_q actually depends on Λ^q: $d_q = d_q(\Lambda^q)$. Since the total $O(p^4)$ correction in the denominator of (30) should be independent of the cutoff Λ^q, d_q for different values of Λ^q varies according to

$$d_q(\Lambda^q) = d_q(\Lambda'^q) - 3\log\left(\frac{\Lambda^q}{\Lambda'^q}\right)^2 . \tag{34}$$

To compare these relations with our results, we fit $\langle\pi^+\pi^0|Q_+|K^+\rangle_{ours}$ as a function of M_π^2 to the form (33). Employing data for which the value of M_π does not exceed the cutoff, we find $d_q(1\mathrm{GeV})/(4\pi)^2 \approx 0.015$ and $d_q(770\mathrm{MeV})/(4\pi)^2 \approx 0.025$. The difference $d_q(1\mathrm{GeV})/(4\pi)^2 - d_q(770\mathrm{MeV})/(4\pi)^2 \approx -0.01$ is in good agreement with the value $-3\log\left(1\mathrm{GeV}/770\mathrm{MeV}\right)^2/(4\pi)^2 = -0.0099$ expected from (34). These results show that the uncertainties associated with d_q can be removed by a chiral extrapolation of our amplitude to the chiral limit $M_\pi = 0$.

A further consequence of (33) is that a correction due to the $O(p^4)$ term d in the full theory remains even after taking the limit $M_\pi \to 0$ in our results. In order to examine the magnitude of this uncertainty, we use an estimate $d(\Lambda^{cont})/(4\pi)^2 = 0.003(14)$ at $\Lambda^{cont} = m_\eta$ from a phenomenological analysis [19]. In view of the formula

$$d(\Lambda^{cont}) = d(\Lambda'^{cont}) - 29.57 \cdot \log\left(\frac{\Lambda^{cont}}{\Lambda'^{cont}}\right)^2 \tag{35}$$

obtained from (30) and (31), this leads to a value $d(770\mathrm{MeV})/(4\pi)^2 \approx -0.12$ and $d(1\mathrm{GeV})/(4\pi)^2 \approx -0.22$. These values imply that the physical decay amplitude is 10% lower than our results for $\Lambda^{cont} = 770\mathrm{MeV}$, and 20% for $\Lambda^{cont} = 1\mathrm{GeV}$. This provides an explanation of a discrepancy of about 10% observed in Figs. 5 and 6 between the values of $\langle\pi^+\pi^0|Q_+|K^+\rangle_{ours}$ calculated with $\Lambda^{cont} = 770\mathrm{MeV}$ and $1\mathrm{GeV}$. Let us add a remark that the values of d estimated above for $\Lambda^{cont} = 770\mathrm{MeV}$ and $1\mathrm{GeV}$ is an order of magnitude larger compared to those of d_q for the quenched theory.

We find from this analysis that including the correction due to the $O(p^4)$ coupling constants is possible if an accurate value of d is known from phenomenological studies. Since this is not yet the case [19], we shall not pursue this point further here, leaving the correction as a source of uncertainty in our final results.

The amplitude obtained from $\langle\pi^+\pi^0|Q_+|K^+\rangle_{ours}$ by a chiral extrapolation to the limit $M_\pi = 0$ is listed in Table III for several choices of the cutoff and the operator matching

point q^*. In the results in Table III, the systematic error due to the matching scale q^* is about 10%. Statistical errors are larger (about 20%), mainly due to a linear extrapolation to the chiral limit. Within these uncertainties and that of 10–20% due to the d term discussed above, the values in Table III are consistent with the experiment $10.4 \times 10^{-3}\text{GeV}^3$.

V. B_K FROM THE $K^+ \to \pi^+\pi^0$ AMPLITUDE

The $\Delta S = 2$ four-quark operator defined by

$$O_{\Delta S=2} = \bar{s}\gamma_\mu(1-\gamma_5)d\ \bar{s}\gamma_\mu(1-\gamma_5)d \tag{36}$$

belongs to the same **27** representation as the operator Q_4 which is the $[\mathbf{27}, \Delta I = 3/2]$ part of Q_+. As a consequence one can obtain the K meson B parameter B_K from the $K^+ \to \pi^+\pi^0$ amplitude using CHPT. The non-vanishing component of the tensor R^{ij}_{kl} in (25) for this operator is given by $R^{22}_{33} = 1$.

The one-loop relation in CHPT for quenched QCD for the unphysical degenerate case has been obtained by Golterman and Leung [9],

$$B_K = \frac{1}{\frac{8}{3}F_K} \cdot \frac{3 \cdot \langle \pi^+\pi^0 | Q_+ | K^+ \rangle}{\frac{3}{\sqrt{2}} \cdot M_\pi^2 (1 + R + d_q)} \tag{37}$$

with the one-loop correction R given by

$$R = \frac{M_\pi^2}{(4\pi F_\pi)^2}\Big[3\log(\frac{M_\pi}{\Lambda^q})^2 + F(M_\pi aL)\Big]\ . \tag{38}$$

Here F_K and F_π denote the K and π meson decay constants in the quenched theory, and the other notations are the same as those in (30–32).

Our procedure for calculating B_K from (37) is essentially the same as for the $K^+ \to \pi^+\pi^0$ amplitude including the operator matching procedure, although the coefficient function C_+ is absent in the present case. In Figs. 7 and 8 we plot $B_K(2\text{GeV})$ obtained from the $K^+ \to \pi^+\pi^0$ decay amplitude with tree and one-loop CHPT. We set $F_K = 160\text{MeV}$ and $F_\pi = 132\text{MeV}$ in (37) and (38). The one-loop CHPT effect and the cutoff dependence for a small M_π^2 region are small compared with those for the decay amplitude. At the physical K meson mass $M_\pi^2 = 0.246\text{GeV}^2$ B_K takes almost the same value for different choices of Λ^q and the lattice size. In Table IV the average of the two data points with the smallest M_π is tabulated. Our results, $B_K = 0.581(56) - 0.663(67)$ are consistent with the JLQCD value $B_K(2\text{GeV}) = 0.68(11)$ [20] obtained at the same coupling constant $\beta = 6.1$ through a calculation of the $K^0 - \overline{K}^0$ matrix element of the $\Delta S = 2$ operator employing chiral Ward identities for determining the mixing coefficients.

A direct calculation of B_K with the Wilson quark action has the complication that the operator mixing problem of the $\Delta S = 2$ operator has to be solved non-perturbatively, which causes large statistical errors. In contrast, the Q_+ operator does not mix with other operators as mentioned in section III B. Therefore, statistical errors of B_K obtained from the $K^+ \to \pi^+\pi^0$ amplitude is smaller. Theoretical uncertainties associated with the use of CHPT, however, are large in this approach that offsets the advantage of the present method. In any case, our calculation, albeit with a significant error, provides an independent check for B_K for the Wilson quark action obtained with the chiral Ward identity procedure, and also supports the validity of CHPT.

VI. CONCLUSIONS

In this article we have reported results of a study of the $K^+ \to \pi^+\pi^0$ decay amplitude in quenched lattice QCD. With a set of high statistics simulations we have found that the results show sizable finite-size effects, which, however, are consistent with those predicted by a recent one-loop calculation of CHPT. We have furthermore seen that a meson mass dependence which remains after inclusion of the one-loop corrections of CHPT in the prediction for the decay amplitude is due to effects of the $O(p^4)$ contact terms in the quenched theory. Making an extrapolation to the chiral limit to remove these effects, we have found $8.9(1.7) \times 10^{-3} - 11.4(1.5) \times 10^{-3}\mathrm{GeV}^3$ for the physical value of the decay amplitude, depending on the choice of the cutoff parameter of CHPT. These values are consistent with experiment ($10.4 \times 10^{-3}\mathrm{GeV}^3$).

The present result may be compared to those of the previous studies [2,4] which gave decay amplitudes roughly twice larger than experiment. Our smaller value originates from the two effects, one-loop corrections as also noted by Golterman and Leung in their reanalysis of the old results, and a decrease of the amplitude toward smaller values of M_π.

As a further application of the one-loop formula, we have calculated the B_K parameter, and found that it is consistent with a recent direct calculation for $K^0 - \overline{K}^0$ mixing.

The encouraging results we have obtained, however, should be taken with several reservations. The value of the $K^+ \to \pi^+\pi^0$ decay amplitude estimated in the chiral limit suffers from uncertainties of 10–20% due to the $O(p^4)$ contact terms of the full theory, because the phenomenological estimate available is not very accurate. A sizable finite-size correction of 30−40%, while consistent with the one-loop prediction of CHPT, raises the question whether ignoring higher order corrections can be justified. Furthermore, various constants of CHPT, in particular the coefficient α_{27}, may differ between the quenched and full theories, and we have no way of estimating or correcting the difference. Reliability of CHPT for calculating unphysical amplitudes could also be an issue. Reducing these sources of uncertainties, especially those related to quenching and better controlling finite-size effects would require a difficult task of carrying out simulations in full QCD on a physically large lattice.

ACKNOWLEDGMENT

We thank Maarten Golterman for informative correspondence on his results for the decay amplitude from chiral perturbation theory. This work is supported by the Supercomputer Project (No. 97-15) of High Energy Accelerator Research Organization (KEK), and also in part by the Grants-in-Aid of the Ministry of Education (Nos. 08640349, 08640350, 08640404, 09246206, 09304029, 09740226).

REFERENCES

[1] M. B. Gavela, L. Maiani, S. Petrarca, G. Martinelli, and O. Pene, Phys. Lett. **211B**, 139, (1988); G. Martinelli, Nucl. Phys. **B** (Proc. Suppl.) **17**, 523, (1990).

[2] C. Bernard and A. Soni, Nucl. Phys. **B** (Proc. Suppl.) **9** , 155, (1989); C. Bernard and A. Soni, Nucl. Phys. **B** (Proc. Suppl.) **17**, 495, (1990); C. Bernard, in *From Actions to Answers, Proc. of the 1989 TASI School*, eds. T. De Grand and D. Toussaint (World Scientific, Singapore, 1990).

[3] G. Kilcup, Nucl. Phys. **B** (Proc. Suppl.) **17**, 533, (1990); S. R. Sharpe, Nucl. Phys. **B** (Proc. Suppl.) **20**, 429, (1991).

[4] M. B. Gavela, L. Maiani, S. Petrarca, F. Rapuano, G. Martinelli, P. Pene and C. Sachrajda, Nucl. Phys. **B306**, 677, (1988).

[5] JLQCD Collaboration, unpublished.

[6] L. Miani and M. Testa, Phys. Lett. **B245**, 585, (1990).

[7] See, *e.g.*, G.P. Lepage, Nucl. Phys. **B** (Proc.Suppl.) **26**, 45, (1992); P. Mackenzie, Nucl. Phys. **B** (Proc.Suppl.) **34**, 35, (1994); A. Kronfeld, Nucl. Phys. **B** (Proc.Suppl.) **34**, 415, (1994) and references cited in theirs.

[8] G.P. Lepage and P.B. Mackenzie, Phys. Rev. **D48**, 2250, (1993).

[9] M.F.L. Golterman and K. C. Leung, Phys. Rev. **D56**, 2950, (1997).

[10] JLQCD Collaboration (S. Aoki *et al.*), Nucl. Phys. **B** (Proc. Suppl.) **53**, 355, (1997); in preparation.

[11] M. Lüscher, Comm. Math. Phys. **105**, 153, (1986).

[12] S.R. Sharpe, R. Gupta, and G.W. Kilcup, Nucl. Phys. **B383**, 309, (1992).

[13] R. Gupta, A. Patel, and S.R. Sharpe, Phys. Rev. **D48**, 388, (1993).

[14] M. Fukugita, Y. Kuramashi, H. Mino, M. Okawa, and A. Ukawa, Phys. Rev. **D52**, 3003, (1995).

[15] G. Martinelli, Phys. Lett. **141B**, 395, (1984).

[16] C. Bernard, T. Draper, and A. Soni, Phys. Rev. **D36**, 3224, (1987).

[17] A. Buras, M. Jamin, and P. H. Weisz, Nucl. Phys. **B347**, 491, (1990); M. Ciuchini, E. Franco, G. Martinelli, and L. Reina, Nucl. Phys. **B415**, 403, (1994).

[18] G. Buchalla, A.J. Buras, and M.E. Lautenbacher, Rev. Mod. Phys. **68**, 1125, (1996).

[19] J. Bijnens, H. Sonoda, and M. B. Wise, Phys. Rev. Lett. **53**, 2367, (1984); J. Kambor, J. Missimer, and D. Wyler, Phys. Lett. **B261**, 496, (1991).

[20] JLQCD Collaboration (S. Aoki *et al.*), Nucl. Phys. **B** (Proc. Suppl.) **53**, 349, (1997); hep-lat/9705035.

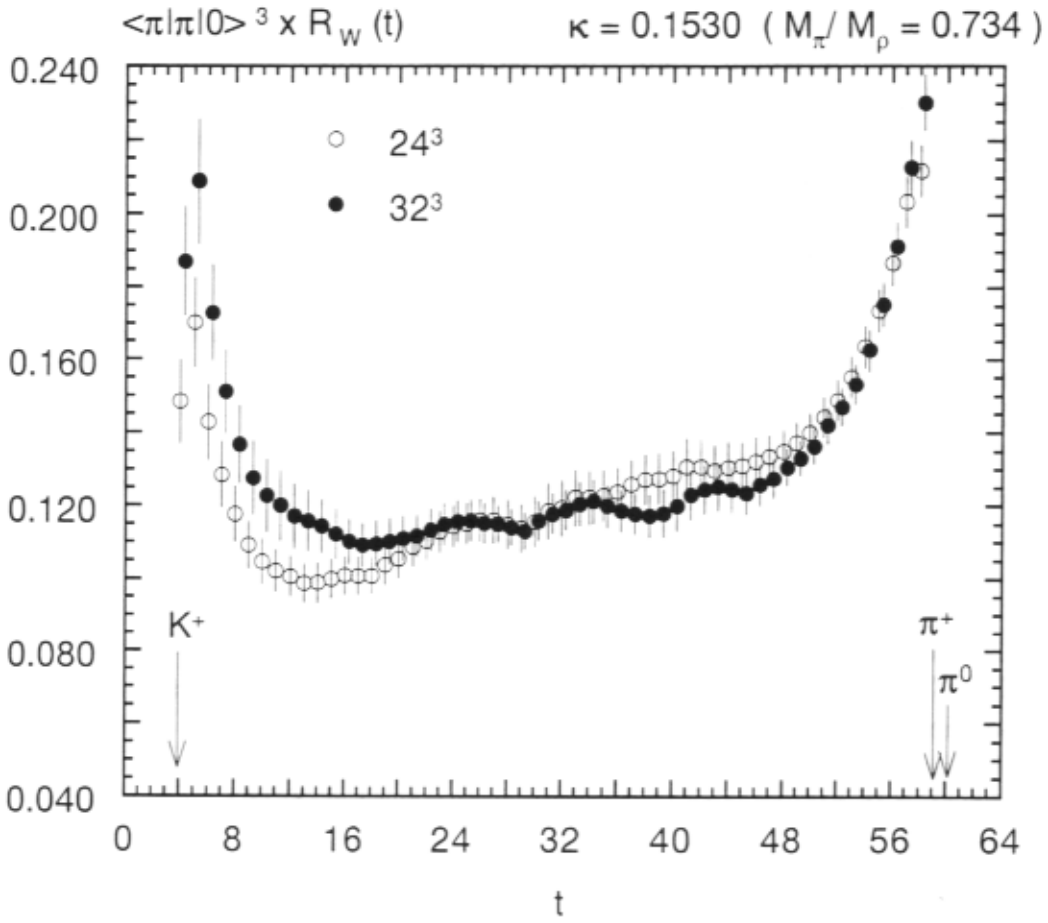

FIG. 1. $\langle\pi|\pi|0\rangle^3 \cdot R_W(t_+, t_0; t; t_K)$ at $\kappa = 0.153$. Open and filled circles refer to data for 24^3 and 32^3 lattices.

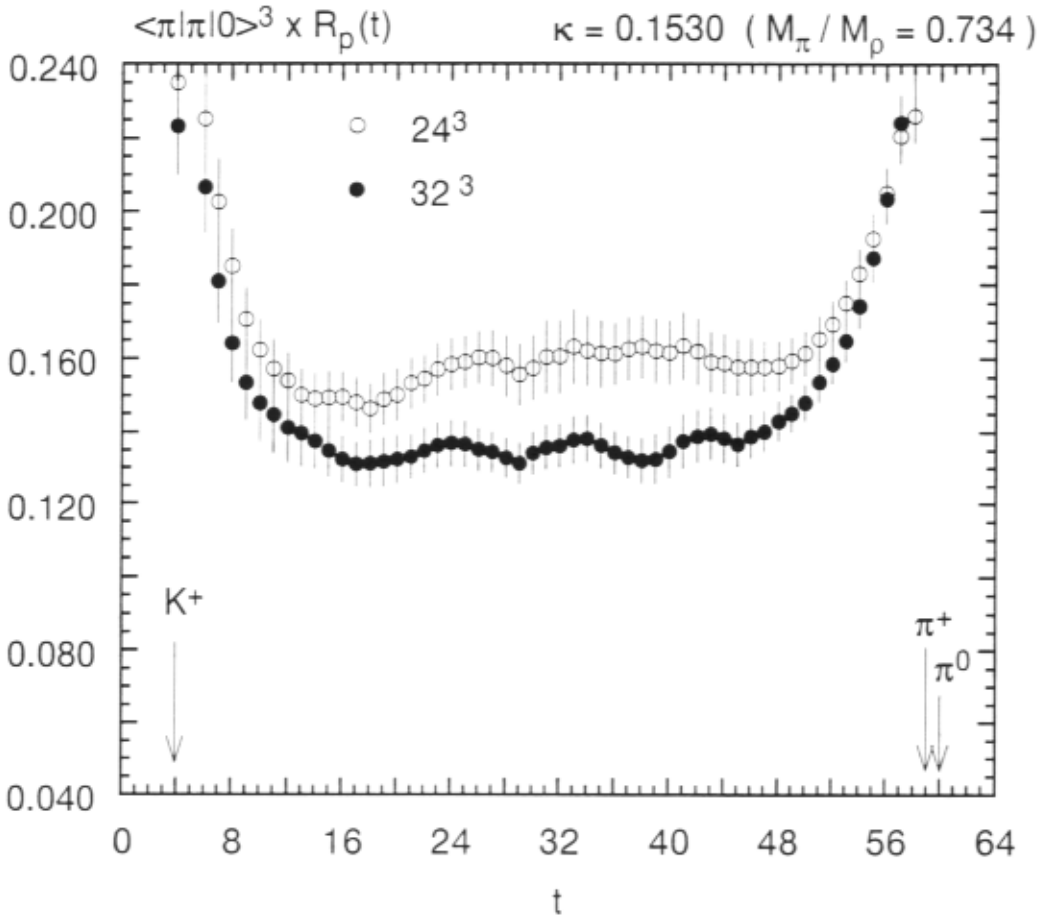

FIG. 2. $\langle\pi|\pi|0\rangle^3 \cdot R_P(t_+, t_0; t; t_K)$ at $\kappa = 0.153$. Open and filled circles refer to data for 24^3 and 32^3 lattices.

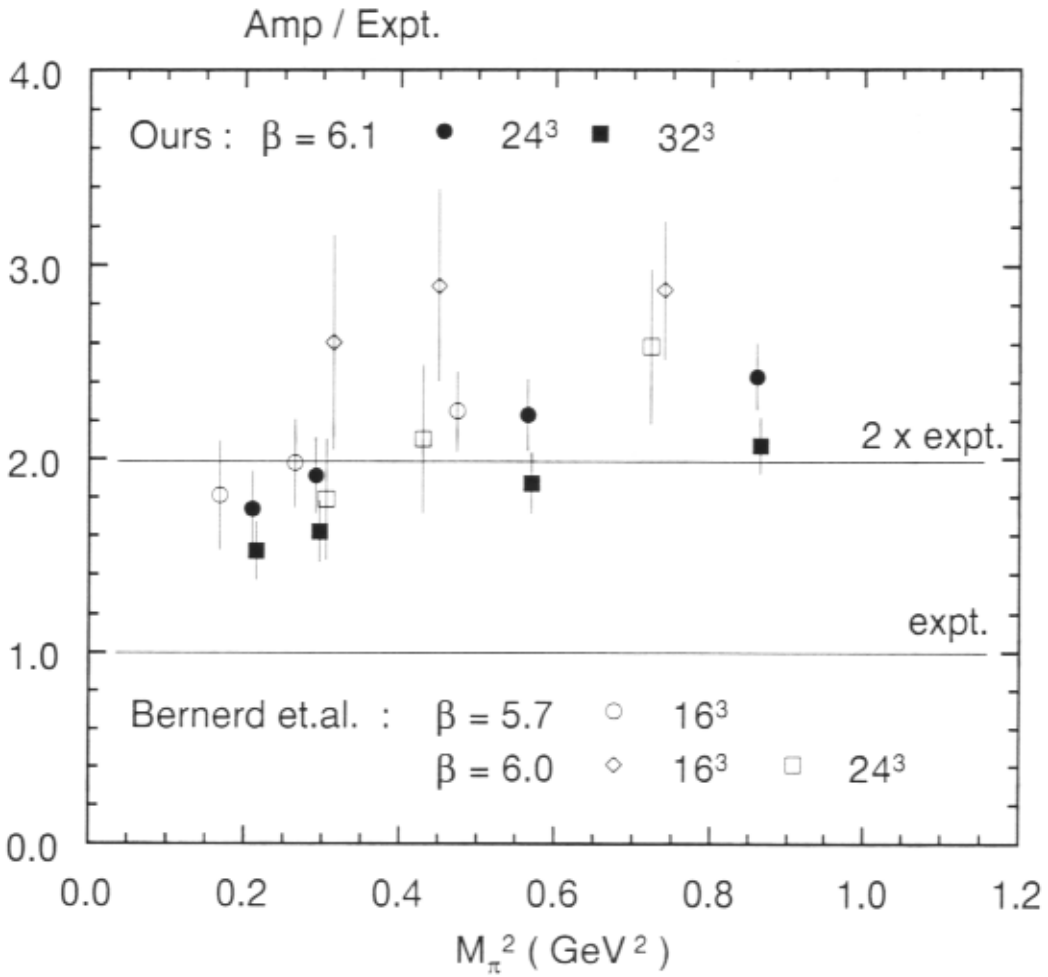

FIG. 3. Comparison of our results for $C_+ \cdot \langle \pi^+\pi^0 | Q_+ | K^+ \rangle$ normalized by the experimental value obtained with tree-level CHPT relation (28) for $q^* = \pi/a$ at $\beta = 6.1$ with those of previous work [2] at $\beta = 6.0$ and 5.7. Results are plotted as a function of lattice meson mass M_π^2. Traditional $\sqrt{2\kappa}$ normalization is employed for quark fields and tadpole-improvement is not applied in the renormalization factor.

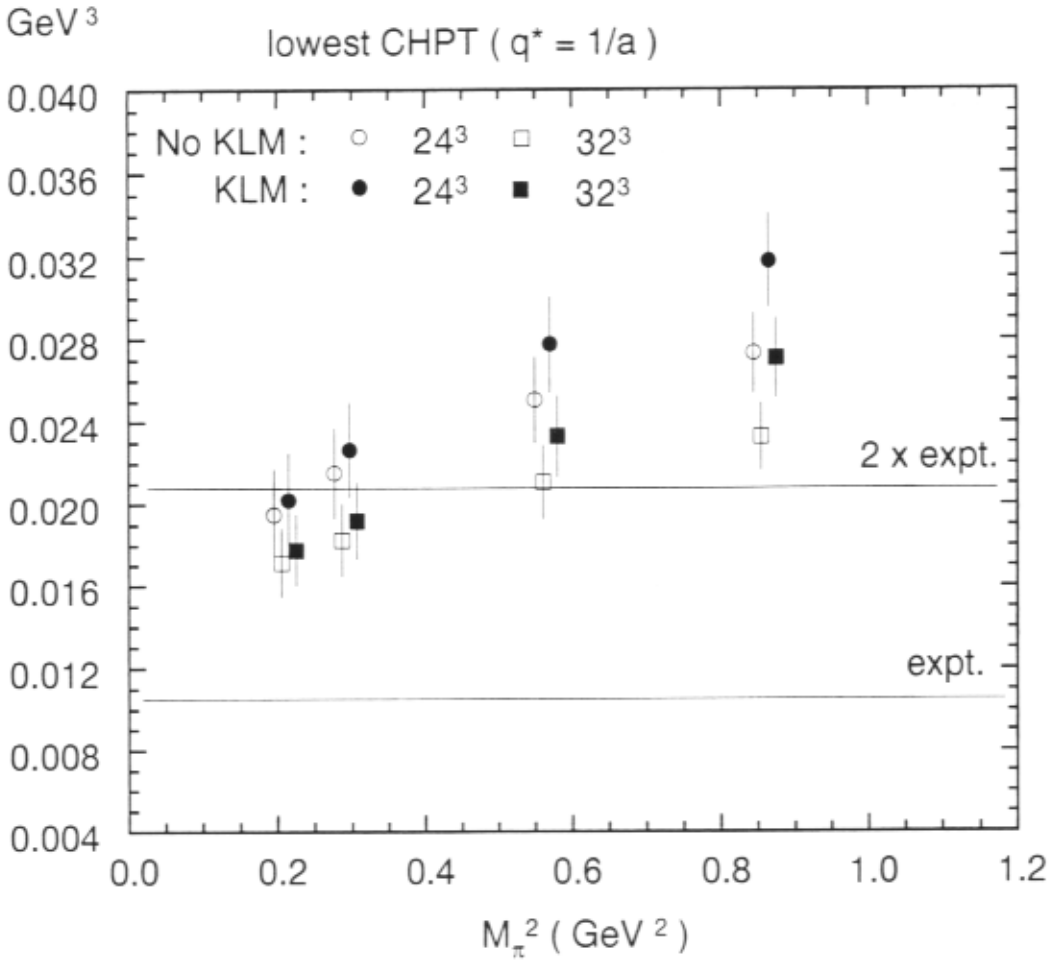

FIG. 4. Decay amplitude $C_+ \cdot \langle \pi^+\pi^0|Q_+|K^+\rangle$ for $q^* = 1/a$ as a function of lattice meson mass M_π^2 for tree-level CHPT. Circles and squared refer to decay amplitude obtained on a 24^3 and 32^3 lattice. Open symbols correspond to the traditional $\sqrt{2\kappa/2\kappa_c}/2$ normalization factor of Wilson quark fields, while filled symbols are for the KLM normalization.

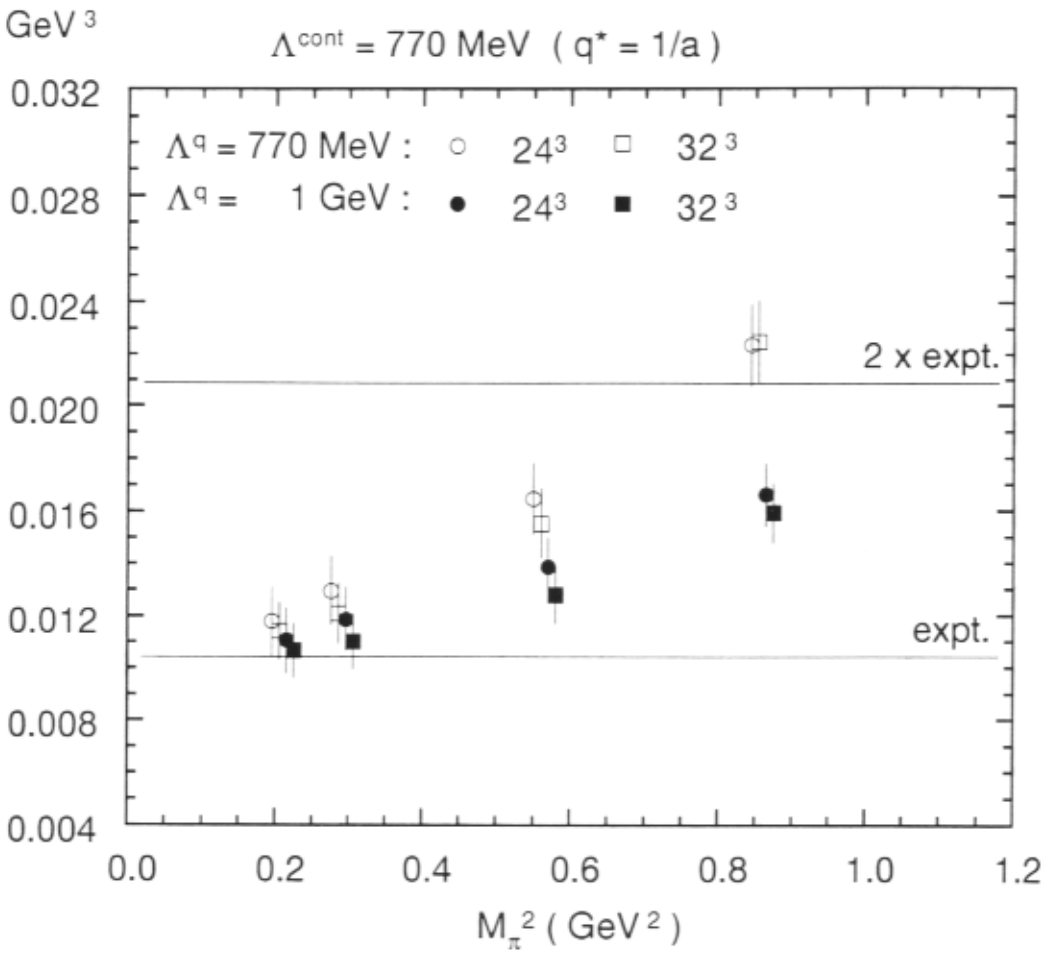

FIG. 5. Decay amplitude $C_+ \cdot \langle \pi^+\pi^0|Q_+|K^+\rangle$ for $q^* = 1/a$ obtained with one-loop CHPT for $\Lambda^{cont} = 770\text{MeV}$ plotted as a function of M_π^2. Circles and squares refer to data for 24^3 and 32^3 spatial sizes. Open symbols are for $\Lambda^q = 770\text{MeV}$ and filled symbols for $\Lambda^q = 1\text{GeV}$.

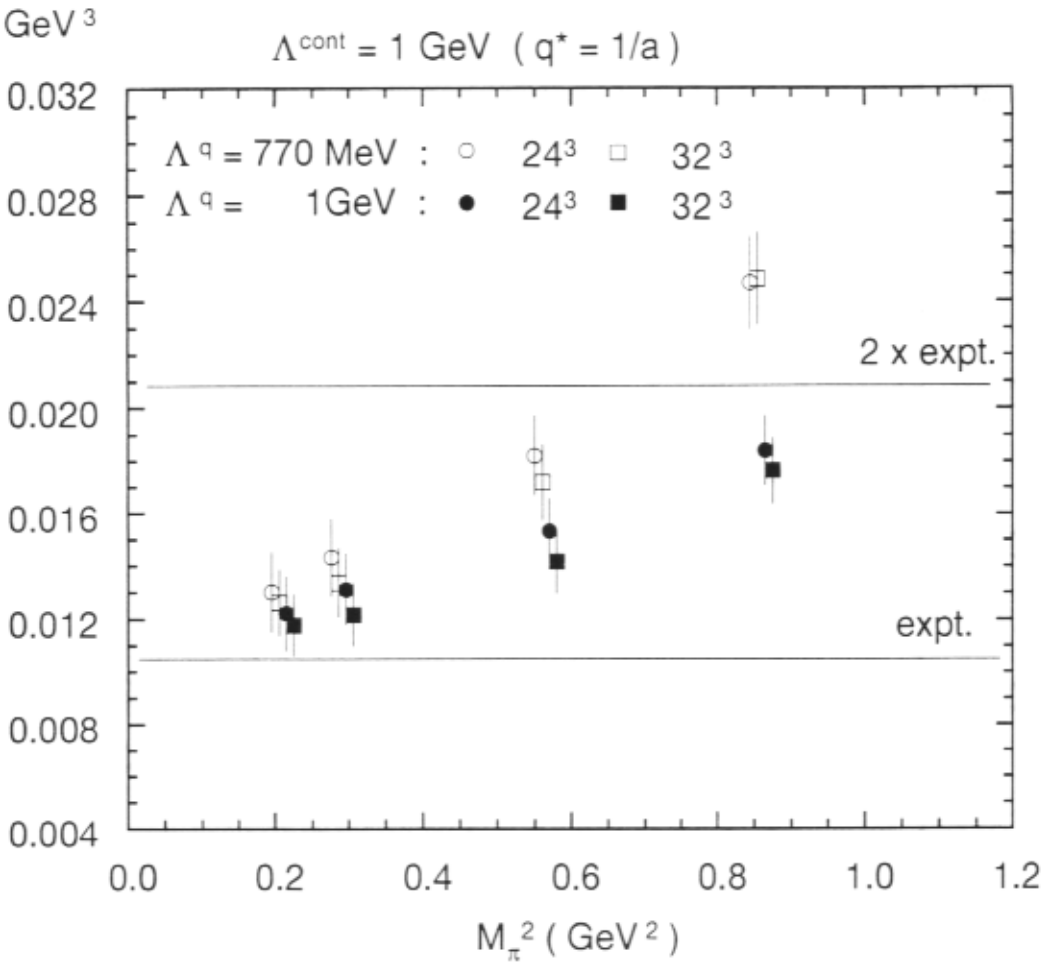

FIG. 6. Decay amplitude $C_+ \cdot \langle \pi^+\pi^0|Q_+|K^+\rangle$ for $q^* = 1/a$ as a function of M_π^2 obtained with one-loop CHPT for $\Lambda^{cont} = 1$GeV. Meaning of symbols are the same as in Fig. 5.

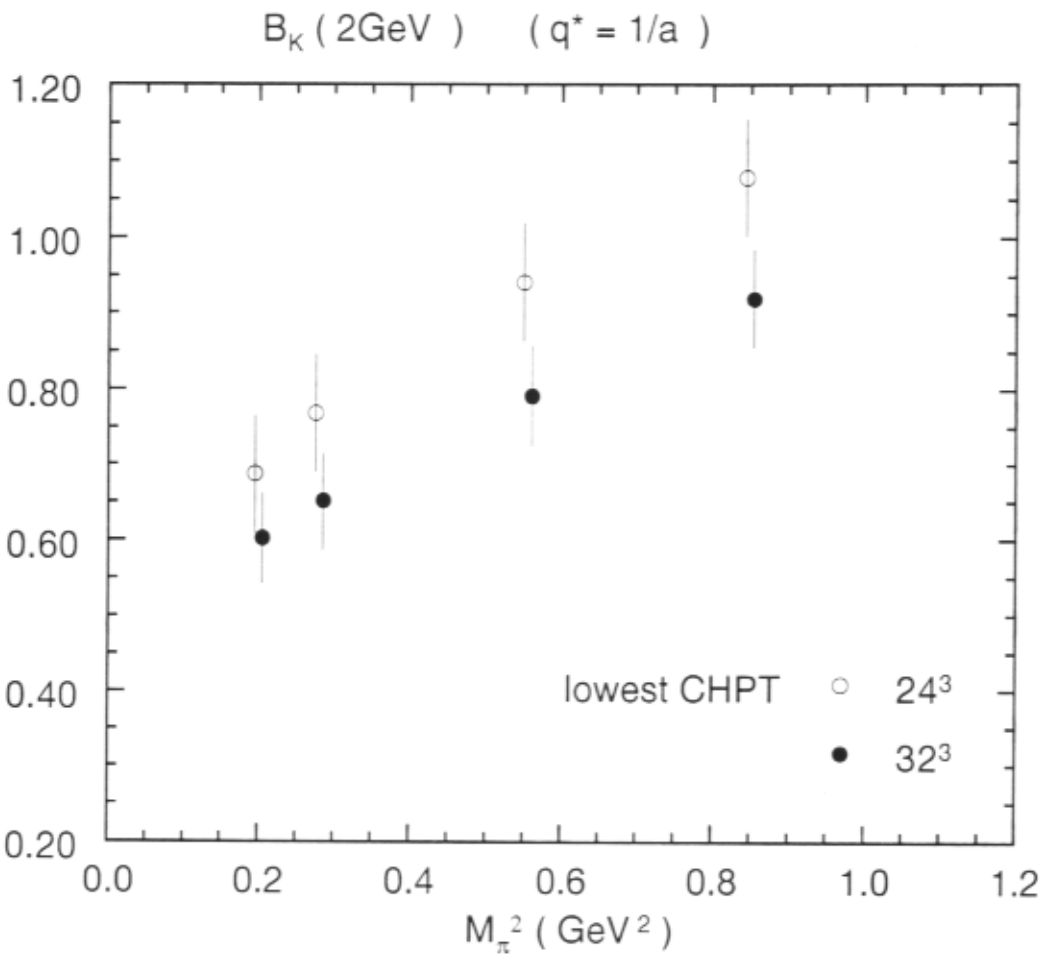

FIG. 7. $B_K(2\text{GeV})$ for $q^* = 1/a$ obtained from $K^+ \to \pi^+\pi^0$ decay amplitude as a function of M_π^2 obtained with tree level CHPT. Circles and squares refer to data for 24^3 and 32^3 spatial sizes.

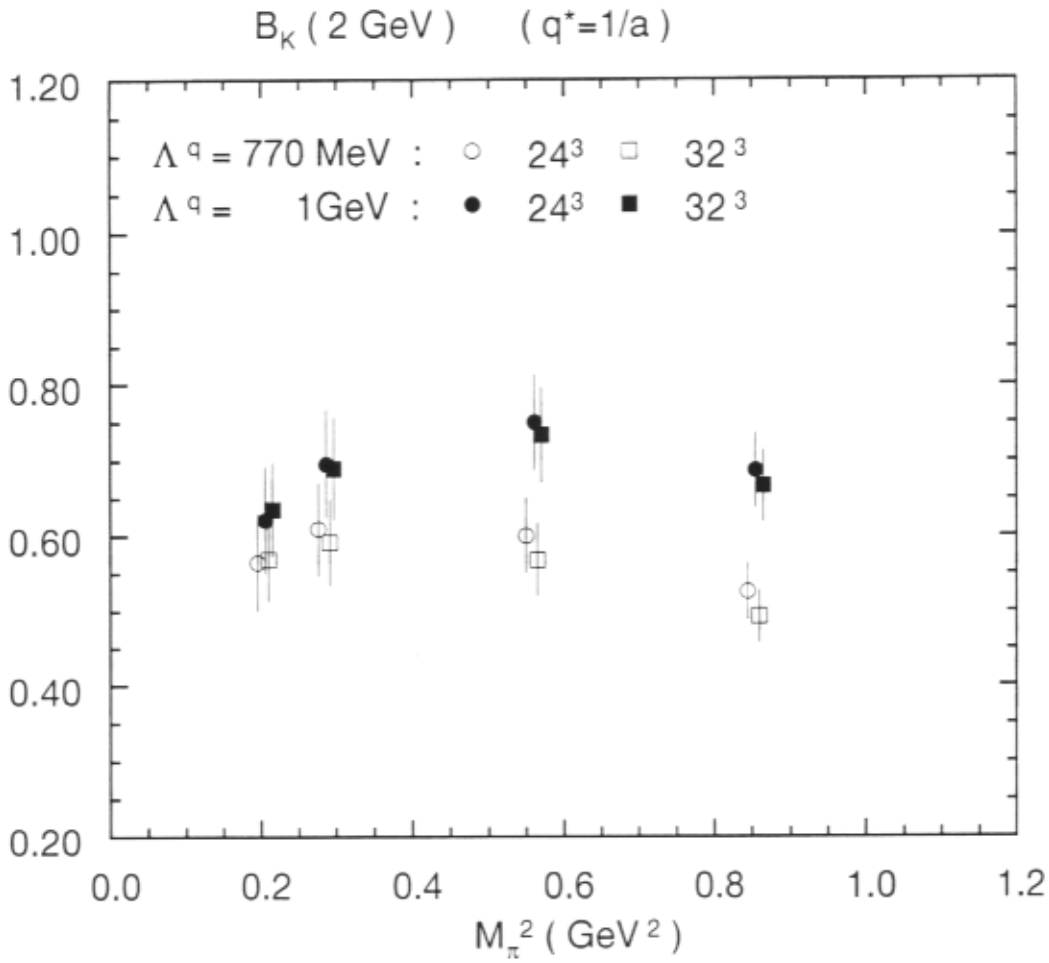

FIG. 8. $B_K(2\text{GeV})$ for $q^* = 1/a$ obtained from $K^+ \to \pi^+\pi^0$ decay amplitude as a function of M_π^2 obtained with one-loop CHPT for $\Lambda^q = 770\text{MeV}$ and 1GeV. Circles and squares refer to data for 24^3 and 32^3 spatial sizes. Open symbols are for $\Lambda^q = 770\text{MeV}$ and filled symbols for $\Lambda^q = 1\text{GeV}$.

TABLES

κ	aM_π	$a\Delta$ (10^{-3})	$\langle\pi^+\pi^0\|Q_+\|K^+\rangle$ from R_W	from R_P
$L = 24$				
0.1520	0.3440(14)	7.9(1.7)	0.261(20)	0.271(19)
0.1530	0.2776(17)	8.6(2.0)	0.151(14)	0.160(13)
0.1540	0.1967(19)	9.3(2.9)	0.0617(81)	0.0680(69)
0.1543	0.1653(21)	8.6(3.6)	0.0382(58)	0.0434(49)
$L = 32$				
0.1520	0.3459(10)	3.6(1.4)	0.229(17)	0.234(16)
0.1530	0.2784(11)	4.2(1.5)	0.132(13)	0.135(11)
0.1540	0.1914(13)	5.7(2.1)	0.0565(71)	0.0573(55)
0.1543	0.1651(15)	7.1(2.8)	0.0383(55)	0.0380(37)

TABLE I. The mass shift $\Delta = M_{\pi\pi} - 2M_\pi$ and $\langle\pi^+\pi^0|Q_+|K^+\rangle$ from R_W and R_P. Here we assume $S_W = S_P = 1$. These value are obtained by a single exponential fit over $t = 18 - 46$ for R_W and by a constant fit over $t = 22 - 42$ for R_P.

k^*(GeV)	$q^* = 1/a$	$q^* = \pi/a$
0.700	0.759038	0.830913
1.000	0.761556	0.833670
1.500	0.765198	0.837657
2.000	0.768126	0.840863

TABLE II. Values of $D(2\text{GeV}, k^*, q^*)$ for $\Lambda^{(4)}_{\overline{\text{MS}}} = 215\text{MeV}$ and $\Lambda^{(0)}_{\overline{\text{MS}}} = 293\text{MeV}$.

Λ^{cont} (GeV)	Λ^q (GeV)	$C_+ \cdot \langle\pi^+\pi^0\|Q_+\|K^+\rangle(\times 10^{-3}\text{GeV}^3)$ 24^3 $q^* = 1/a$	24^3 $q^* = \pi/a$	32^3 $q^* = 1/a$	32^3 $q^* = \pi/a$
0.77	0.77	9.3(1.9)	10.2(2.1)	8.9(1.7)	9.7(1.9)
0.77	1.0	9.4(1.3)	10.3(1.4)	8.8(1.1)	9.6(1.2)
1.0	0.77	10.3(2.1)	11.3(2.3)	9.8(1.9)	10.7(2.1)
1.0	1.0	10.4(1.4)	11.4(1.5)	9.7(1.2)	10.6(1.3)

TABLE III. Results of linear extrapolation of $C_+ \cdot \langle\pi^+\pi^0|Q_+|K^+\rangle$ to $M_\pi^2 = 0$. For $\Lambda^q = 770\text{MeV}$ fits are made with three points with smaller M_π as M_π of the forth point exceeds the cutoff. Statistical and extrapolation errors are combined. The experimental value is $10.4 \times 10^{-3}\text{GeV}^3$.

	tree	$\Lambda^q = 0.77$GeV	$\Lambda^q = 1$GeV
24^3	0.728(78)	0.587(64)	0.659(71)
32^3	0.627(63)	0.581(58)	0.663(67)

TABLE IV. $B_K(2\text{GeV})$ at physical K meson mass $M_\pi = 496$MeV obtained from the $K^+ \to \pi^+\pi^0$ amplitude. The row "tree" refers to result with lowest CHPT and others are obtained by one-loop CHPT for $\Lambda^q = 0.77$GeV and 1GeV.